An ATM-PPM1D Circuit Controls the Processing and Restart of DNA Replication Forks

Yiting Cao[1#], Yingzheng Wang[1#], Jumana Badar[1#], Khoula Jaber[1], Vitor Marcel Faça[2], Tyler C. Huang[1], Eliz Çelik[1], and Marcus B. Smolka[1*]

[1] Department of Molecular Biology and Genetics, Weill Institute for Cell and Molecular Biology, Cornell University, Ithaca, NY, 14850, USA

[2] Department of Biochemistry and Immunology and Cell-Based Therapy Center, Ribeirao Preto Medical School, University of Sao Paulo, Ribeirao Preto, SP, 14049-900, Brazil

# These authors contributed equally to this work.

*To whom correspondence should be addressed: Marcus B. Smolka, e-mail: mbs266@cornell.edu

ABSTRACT

In response to DNA replication stress, DNA damage signaling kinases inhibit origin firing and promote the remodeling and stabilization of replication forks, leading to a systemic reduction in DNA synthesis, which collectively protects genomic integrity. Little is understood about the regulatory mechanisms of replication stress recovery, including the mechanisms involved in the restart of stalled replication forks. Here, we identify the oncogenic phosphatase PPM1D/WIP1 as a regulator of replication fork restart. During recovery from replication stress, PPM1D prevents excessive MRE11- and DNA2-dependent nucleolytic degradation of stalled forks. Loss of PPM1D function leads to defects in RAD51 recruitment to chromatin and impairs RAD51-dependent fork restart. Phosphoproteomic analysis reveals that PPM1D regulates a network of ATM substrates, several of which are phosphorylated at an S/T-Q-$(E/D)^n$ motif. Strikingly, inhibition of ATM suppresses the deleterious consequences of impaired PPM1D function at replication forks, enabling timely fork restart. The dominant effect of ATM hyper-signaling in suppressing fork restart occurs, in part, through the excessive engagement of 53BP1 and consequent RAD51 antagonization. These findings uncover a new mode of ATM signaling responding to fork stalling and highlight the need for PPM1D to restrain ATM signaling and facilitate proper fork restart.

39 **INTRODUCTION**

40

41 DNA replication occurs within a highly complex and dynamic genomic landscape. The
42 progression of DNA replication forks is often slowed or impeded by various obstacles, such as
43 DNA lesions or adducts, secondary DNA structures, transcriptional intermediates, compacted
44 chromatin, and the shortage of nucleotides and other essential replication factors (*1*, *2*). When
45 replication forks stall, they become vulnerable structures prone to degradation by nucleases,
46 which can lead to the extensive single-stranded DNA (ssDNA) accumulation and/or the
47 formation of double-stranded breaks (DSBs) (*3*). The ability of cells to maintain the integrity of
48 stalled replication forks largely relies on the ATR kinase, a member of the phosphatidylinositol
49 3-kinase–related kinase (PIKK) family, which senses the exposure of ssDNA at replication forks
50 (*4*). Upon fork stalling, ATR and its downstream effector CHK1 suppress late origin firing to
51 prevent the exhaustion of key replication factors, including nucleotides, replication protein A
52 (RPA), and the RFC/PCNA complex (*5*, *6*). In parallel, ATR signaling restrains the activity of
53 nucleases, such as MRE11, EXO1, and MUS81, to limit excessive fork processing (*7*–*9*). Cells
54 also rely on structural remodeling of replication forks to avoid nucleolytic degradation (*10*). For
55 instance, a replication fork regresses into a four-way DNA junction, known as fork reversal,
56 allowing nascent DNA strands to be stabilized by protective factors such as RAD51, BRCA1,
57 and BRCA2 (*3*, *11*). This reversal process is catalyzed by DNA translocases, including
58 SMARCAL1, HLTF, and ZRANB3 (*12*), and is tightly regulated by the DNA damage response
59 kinases ATR and DNA-PKcs (*13*, *14*).

60

61 While fork reversal and protection are important for stabilizing replication forks, the restart of
62 stalled replication forks is essential for the timely completion of DNA replication and the
63 preservation of genomic integrity (*15*). Stalled forks that undergo regression can be restarted by
64 branch migration, via the RECQ1 helicase, which is considered the primary choice for fork

65 restart given the minimal chance for error-prone DNA processing (*16*). Alternatively, reversed
66 forks can be restarted through regulated processing of the regressed ends by helicases and
67 nucleases, such as WRN and DNA2, enabling RAD51-mediated homologous recombination
68 (HR) transactions for restoring a functional replication fork (*17*). In addition, forks that collapse
69 may undergo HR-mediated repair transactions to restore a functional fork, albeit with an
70 increased risk of initiating mutagenic processes such as break-induced replication (BIR) (*18*).
71 Engagement of NHEJ-mediated repair into fork-associated DSBs also has the potential of
72 generating deleterious outcomes, such as chromosomal translocations, especially when single-
73 ended DSBs are generated (*19*, *20*). Moreover, processes that prevent the stalling of a
74 replication fork, such as PrimPol-mediated repriming or translesion synthesis, can mitigate the
75 potential deleterious outcomes associated with stalled or collapsed forks, although they also
76 introduce mutations and other genomic instabilities (*21*). Overall, the ability of cells to restart
77 replication forks in a regulated and error-free manner is crucial to protect genome integrity upon
78 replication stress. Since replication fork restart mechanisms need to counteract the mechanisms
79 that stabilize stalled forks, including fork reversal and inhibition of nucleolytic processing, cells
80 must tightly control the balance of fork-stabilizing and fork-restarting mechanisms during
81 replication stress recovery.
82
83 While ATR is the central kinase in the response to stalled forks, the other PIKKs, ATM and
84 DNA-PKcs, were also reported to engage in the response to various forms of replication stress.
85 For example, in response to replication stress induced by the B-family DNA polymerase inhibitor
86 aphidicolin, ATM was shown to phosphorylate several proteins, including H2AX, Claspin,
87 BRCA1, MCM3, MCM6 and RIF1 (*22*), in a manner dependent on RAD18, WRNIP1, and
88 ATMIN (*23*). Consistent with its major role in the double-strand break (DSB) response, ATM is
89 robustly activated by agents that cause replication fork-associated DSBs, such as the
90 topoisomerase inhibitors camptothecin and etoposide (*24*, *25*). Differences in the cellular

91 response to stalled versus broken replication forks have been characterized at the proteomic
92 level, which revealed a role for ATM in promoting HR-mediated repair specifically at broken
93 forks by impairing recruitment of the anti-resection BRCA1-A complex (*25*). DNA-PKcs, which
94 also has canonical roles in the DSB response, was shown to be recruited to both ongoing and
95 stalled replication forks, where it mediates drug-induced replication fork reversal and promotes
96 fork stability through mechanisms that remain unknown (*14*, *26–28*).
97
98 Since PIKK signaling halts core cellular processes such as DNA replication and cell cycle
99 progression (*29*, *30*), mechanisms for the deactivation of PIKK signaling must be in place to
100 enable proper recovery from replication stress. Multiple phosphatases have been implicated in
101 antagonizing PIKK signaling, including PP1, PP2A, PPM1G and PPM1D (*31–33*). The
102 phosphatase PPM1D (protein phosphatase Mn^{2+}/Mg^{2+}-dependent 1D) has been shown to play
103 prominent roles in dephosphorylating and antagonizing ATM, p53 and CHK2 (*34–37*). PPM1D is
104 overexpressed in multiple tumor types, including breast, ovarian, and glioblastoma tumors (*38*),
105 which can occur through gene amplification or truncating mutations that remove a degron at its
106 C-terminal domain (*39*, *40*). Elevated PPM1D protein levels counteract DNA damage signaling
107 and are proposed to play a major role in reducing p53-mediated apoptosis (*39*, *41*, *42*). Not
108 surprisingly, PPM1D overexpression has been implicated in chemotherapy resistance (*39*, *43*).
109
110 Here we find that PPM1D/WIP1 is required for the restart of stalled replication forks. Upon
111 recovery from replication stress, PPM1D prevents the excessive nucleolytic degradation of
112 stalled forks. Loss of PPM1D function leads to defects in RAD51 recruitment to chromatin and
113 impairs RAD51-dependent fork restart. Phosphoproteomic analysis reveals that PPM1D
114 regulates a network of proteins involved in ATM signaling, several of which are targeted by ATM
115 at an S/T-Q-$(E/D)^n$ motif. Strikingly, inhibition of ATM suppresses the deleterious consequences
116 of impaired PPM1D function at replication forks, enabling timely fork restart. The dominant effect

117 of ATM hyper-signaling in suppressing fork restart occurs through the excessive engagement of
118 53BP1 and consequent RAD51 antagonization. These findings uncover a new mode of ATM
119 signaling responding to fork stalling and highlight the need for PPM1D to limit ATM signaling
120 and enable proper fork restart.
121
122

123 # RESULTS

124

125 **PPM1D is required for proper restart of stalled replication forks**

126 In search for phosphatases required for proper fork restart, we focused on the oncogenic
127 phosphatase PPM1D (PP2Cδ/WIP1), since it was previously shown to antagonize PIKK
128 signaling (*34*, *36*, *44–47*). PPM1D is a monomeric phosphatase for which a potent and selective
129 inhibitor is available (GSK2830371; herein referred to as PPM1Di) (*48*), which allowed us to
130 assess the importance of PPM1D during recovery from replication stress. U2OS cells were
131 treated with hydroxyurea (HU) for 30 minutes, a condition previously reported to promote
132 replication fork stalling without causing fork collapse (*49*). Cells were then washed and released
133 in the presence or absence of PPM1Di, and DNA synthesis was assessed by monitoring the
134 incorporation of the nucleotide analog EdU (Fig. 1a). As shown in Figs. 1a-b, PPM1Di reduced
135 the ability of cells to incorporate EdU, suggesting a defect in replication fork restart and/or origin
136 firing. A similar result was observed in PPM1D-knockout U2OS cells, supporting that the
137 observed effects were not due to off-target inhibitor activity (Figs. 1c and S1a-b). DNA combing
138 assay in U2OS cells revealed that the reduction in EdU incorporation caused by PPM1Di was
139 associated with an increase in stalled forks and a reduction in fork restart (Figs. 1d and S1c).
140 Consistent results were observed using DNA fiber assays in both U2OS and HCT116 cells (Fig.
141 S1f). Additionally, both knockdown and knockout of PPM1D significantly increased the
142 frequency of stalled forks. Notably, in PPM1D knockout cells, siPPM1D neither increases fork
143 stalling nor decreases fork restart, supporting the specificity of the siPPM1D-mediated depletion
144 (Figs. 1e and S1d). PPM1Di did not reduce origin firing (Fig. S1f), consistent with a defect in
145 fork restart being the major cause of the observed reduction in DNA synthesis during recovery
146 from replication stress. This notion is also supported by the additive effect of PPM1Di in
147 combination with the CDC7 inhibitor, an inhibitor of origin firing, in reducing DNA synthesis (Fig.

148 S1g). Moreover, the overall abundance of PPM1D is increased in S-phase cells (Figs. 1f-g),
149 consistent with previously published results (*50*), and supporting a potential role for PPM1D in
150 DNA replication. Taken together, these results reveal a role for PPM1D in the control of
151 replication fork restart.
152
153 **PPM1D prevents the nucleolytic processing of stalled replication forks during replication**
154 **stress recovery**
155 To gain insights into how loss of PPM1D function impairs replication forks during replication
156 stress recovery, we monitored RPA32 foci as a proxy for ssDNA accumulation. U2OS cells were
157 treated with HU for 30 minutes and released in the presence or absence of PPM1D function. As
158 shown in Figs. 2a-d, both PPM1Di and PPM1D knockout caused an increase in RPA32 foci in
159 PCNA-positive cells. We also monitored the accumulation of ssDNA at nascent DNA strands
160 during release from HU arrest using BrdU labeling followed by non-denaturing
161 immunofluorescence and observed a significant increase in nascent ssDNA exposure in cells
162 treated with PPM1Di (Figs. 2e and S2a-b). We interpret the increased BrdU signal on nascent
163 DNA strands as likely originating from ssDNA at regressed replication forks. Consistent with this
164 notion, cells lacking SMARCAL1, a translocase involved in fork reversal, did not exhibit
165 significantly increased levels of RPA32 foci or stalled forks upon PPM1Di treatment during HU
166 release (Figs. 2f-g and S2c). Moreover, inhibition of the nucleases MRE11 or DNA2 suppressed
167 RPA32 foci accumulation (Figs. 2h-i), supporting the model that, upon PPM1Di treatment during
168 HU release, the action of these nucleases generates excessive ssDNA at stalled replication
169 forks. Notably, DNA2 seemed to play a more prominent role, with DNA2i completely rescuing
170 the effect of PPM1Di, consistent with previous reports showing that this is the key nuclease
171 involved in the hyper-processing of reversed replication forks (*17*). Overall, these results point to
172 a role for PPM1D in preventing the aberrant nucleolytic processing of stalled replication forks
173 during recovery from replication stress.

174

175 **PPM1D antagonizes ATM signaling during recovery from fork stalling**

176 To delineate the contribution of PPM1D to signaling downregulation during recovery from
177 replication stress, we compared the phosphoproteomes of mock-treated versus PPM1Di-treated
178 cells during release from HU arrest. The generated dataset was crossed with data from a
179 separate analysis comparing the phosphoproteomes of cells arrested by HU with the
180 phosphoproteome of cells that were HU-arrested and then released, yielding a dataset of
181 10,833 overlapping phosphosites identified in both phosphoproteomic experiments (Fig. 3a,
182 Table S1). PPM1Di caused extensive changes in signaling during replication stress recovery,
183 resulting in at least a two-fold increase in the abundance of about 18% of the phosphorylation
184 events found to be downregulated during release from HU arrest (Figs. 3a-b). While this finding
185 defines PPM1D as a prominent phosphatase acting during replication stress recovery, it also
186 implies that additional phosphatases must contribute to the dephosphorylation of other signaling
187 events downregulated during replication stress recovery. Notably, out of the phosphorylation
188 events upregulated by at least 2-fold upon treatment with PPM1Di, 22.5% contained a
189 phosphorylation event at the SQ/TQ consensus motif (Fig. 3c), suggesting that PPM1D displays
190 some level of selectivity for antagonizing PIKK signaling. Consistent with previous reports, we
191 found that PPM1D displays a preference for targeting phosphorylation at an S/T-Q-$(E/D)^n$ motif
192 (Fig. 3d) (*47*, *51*). Notably, the phosphorylation events at S/T-Q-$(E/D)^n$ motifs most highly
193 regulated by PPM1D included several known substrates of the ATM kinase, such as RAP80,
194 NUMA1, SMC1A, and 53BP1 (*52*–*55*), suggesting that PPM1D plays a prominent role in
195 antagonizing ATM signaling. We confirmed this prediction by monitoring the phosphorylation of
196 KAP1 at serine 824, a well-established ATM substrate within the S/T-Q-$(E/D)^n$ motif (*56*, *57*). As
197 shown in Figs. 3e-g, while PPM1D inhibition during release from HU treatment caused a drastic
198 increase in KAP1 phosphorylation, it led to a more subtle increase in CHK1 phosphorylation,
199 consistent with the model that PPM1D plays a more prominent role in antagonizing ATM

200 signaling compared to ATR signaling. Notably, we did not observe changes in the level of ATM
201 autophosphorylation (Fig. 3h), suggesting that PPM1D acts on ATM downstream substrates as
202 opposed to acting on ATM itself. Overall, our results establish PPM1D as a key phosphatase
203 antagonizing ATM signaling during replication stress recovery.
204

205 **Unrestrained ATM signaling causes aberrant fork processing and fork restart defects**
206 **upon loss of PPM1D function**

207 Since inhibition of PPM1D resulted in the increased phosphorylation of multiple ATM substrates
208 during replication stress recovery, we next tested whether inhibition of ATM could suppress the
209 defects we observed with fork restart and nucleolytic processing. PPM1Di alone did not cause a
210 strong reduction in EdU incorporation when compared to its effect during replication stress
211 release (Fig. S3a). Strikingly, inhibition of ATM during release from HU treatment fully rescued
212 the increased accumulation of RPA32 foci (Figs. 4a-b) and restored EdU incorporation in
213 PPM1Di-treated cells (Figs. 4c-d and S3a). ATMi also rescued the accumulation of stalled forks
214 and fork degradation caused by PPM1Di, as monitored by DNA fiber assays (Figs. 4e-f and
215 S3b-c). Furthermore, inhibition of ATM, but not ATR, was able to rescue the proliferation defect
216 caused by PPM1Di (Fig. 4g), reinforcing the hypothesis that PPM1D plays a key role in
217 selectively antagonizing ATM-dependent signaling. Taken together, these results support a
218 model in which PPM1D dephosphorylates ATM substrates during recovery from replication
219 stress, thereby preventing their toxic accumulation and the consequent hyperactivation of
220 nucleases whose action results in ssDNA accumulation and defects in fork restart.
221

222 **PPM1D controls RAD51 chromatin recruitment and RAD51-mediated fork restart**

223 To better characterize the effects of unrestrained ATM signaling during replication stress
224 recovery, we monitored RAD51, a recombinase protein with separable roles in protecting
225 reversed forks from degradation and mediating fork restart via homologous recombination (*58*).

226 Immunofluorescence-based analysis revealed that the number of RAD51 foci was significantly
227 reduced in cells treated with PPM1Di during recovery from replication stress (Figs. 5a-b). This
228 finding is consistent with a recent report showing that PPM1D inhibition suppresses RAD51 foci
229 formation in DIPG cells, as well as in U2OS cells following exposure to ionizing radiation (*59*,
230 *60*). In addition, chromatin fractionation also revealed a reduction of RAD51 in the chromatin-
231 bound fraction upon PPM1D inhibition during recovery from replication stress (Fig. 5c). We
232 hypothesized that PPM1D promotes RAD51-dependent fork restart during replication stress
233 recovery. To test this, we performed the DNA fiber assay to monitor persistent fork stalling in
234 cells treated with the RAD51 inhibitor B02, in the presence or absence of PPM1Di (Figs. 5d and
235 S4). Consistent with previous reports highlighting the importance of RAD51 for fork restart (*49*),
236 RAD51 inhibition alone increased the incidence of stalled forks. Cells co-treated with RAD51i
237 and PPM1Di during recovery from HU arrest did not display increased incidence of stalled forks
238 compared to cells treated with RAD51i alone. These findings suggest that PPM1D and RAD51
239 function through the same pathway to facilitate fork restart. The degree of fork stalling in
240 RAD51i-treated cells was higher than in PPM1Di-treated cells, congruent with a model whereby
241 PPM1D functions as a regulator of RAD51 roles in ensuring proper fork restart. Such regulation
242 is likely to involve PPM1D's role in antagonizing ATM signaling as inhibition of ATM prevents
243 reduction of RAD51 foci in PPM1D-KO cells (Fig. 5e). Additionally, we observed that PPM1D
244 inhibition caused a rapid increase in 53BP1 foci during the recovery from replication stress, and
245 that the increase was dependent on ATM (Fig. 5f). 53BP1 is a bona-fide ATM target (*61*, *62*)
246 and one of the top PPM1D-regulated targets identified in our phosphoproteomic screen (Fig.
247 3d). Recent studies have shown that 53BP1 counteracts RAD51 loading at replication forks
248 independently of its role in antagonizing resection (*63*). Therefore, we reasoned that the
249 hyperphosphorylation of 53BP1 upon PPM1D inhibition causes its accumulation at stalled
250 replication forks, which in turn counteracts RAD51 engagement, thereby impairing proper fork

251 restart. Consistent with this model, PPM1D inhibition did not cause a decrease in RAD51
252 engagement in 53BP1-KO cells (Fig. 5g).
253
254 **Increased phosphorylation status of ATM targets upon loss of PPM1D is not correlated**
255 **with an increase in detectable DSBs**
256 ATM is canonically activated by DSBs (*64*). However, neutral comet assay did not detect
257 PPM1Di-dependent increase in DSBs within 30 minutes following recovery from replication
258 stress, a time point in which PPM1D inhibition resulted in a significant increase in the ATM-
259 dependent phosphorylation of KAP1 at serine 824 (Figs. 6a-c). These findings suggest that
260 ATM signaling and the observed increases in the phosphorylation status of ATM substrates are
261 independent of DSB formation during early replication stress recovery. Our finding that the
262 autophosphorylation of ATM is not increased during release from replication stress is also
263 consistent with this notion (Fig. 3h). To provide further evidence that PPM1D inhibition is not
264 causing strong induction of DSBs early (~30 minutes) during recovery from replication stress,
265 we engineered a ProKAS biosensor (*65*) containing two sensors that differentiate ATM signaling
266 regulated by PPM1D (ATM-PPM1D sensor) from ATM signaling that is not controlled by PPM1D
267 (ATM sensor) (Figs. 6d-e). As shown in Figs. 6f and S5, CPT robustly increased the
268 phosphorylation of both sensors, consistent with the canonical role of ATM in responding to
269 DSBs. The ATM sensor did not report increased ATM activity during recovery from replication
270 stress, in the absence or presence of PPM1D inhibitor, further supporting the absence of DSB-
271 induced ATM signaling under these conditions. Notably, the ATM-PPM1D sensor reported a
272 drastic increase in ATM signaling upon PPM1D inhibition during recovery from replication
273 stress. These findings with the biosensor are congruent with the model that PPM1D inhibition is
274 not causing DSBs, and suggest that in the context of replication fork stalling and restart, ATM
275 may be activated by alternative DNA structures, such as the nascent DNA ends of reversed
276 forks.

277 **DISCUSSION**

278

279 The ability of cells to restart stalled replication forks is crucial for the faithful completion of DNA
280 replication under conditions of replication stress. Despite its importance, the regulatory
281 mechanisms that govern fork restart remain incompletely understood. Here, we identify the
282 phosphatase PPM1D as a regulator of replication fork recovery. Our findings reveal that
283 attenuation of ATM-mediated signaling is a central function of PPM1D during replication stress
284 resolution. In our working model (Fig. 6g), ATM is activated at stalled forks and phosphorylates
285 substrates such as 53BP1, which in turn interferes with RAD51 loading. Persistent ATM activity
286 antagonizes HR-mediated fork restart and also leads to fork degradation due to reduced
287 RAD51-mediated fork protection. PPM1D counteracts the block in RAD51 loading by
288 dephosphorylating ATM targets. Thus, the ATM–PPM1D axis acts as a dynamic rheostat that
289 modulates ATM signaling at stalled forks to coordinate the balance between fork protection and
290 fork restart.

291

292 A key unresolved question is how PPM1D is recruited to stalled forks. It is possible that the
293 build-up of ATM-dependent phosphorylation events triggers PPM1D recruitment, establishing a
294 feedback mechanism to restrain excessive ATM signaling at forks. Future studies will be
295 needed to define the mechanisms driving PPM1D localization and whether recruitment is
296 influenced by specific post-translational modifications, replisome-associated factors, or fork-
297 associated DNA structures. Moreover, our results suggest that PPM1D primarily acts on ATM
298 substrates rather than directly on ATM itself or ATR substrates. This is consistent with PPM1D's
299 preference for dephosphorylating S/T-Q motifs followed by acidic residues [S/T-Q-(D/E)n
300 motifs], a motif also preferred by ATM (*66*).

While ATM canonically responds to DSBs, our work suggests that ATM can also respond to replication stress independently of DSB formation. Under conditions of PPM1D inhibition, we observe elevated ATM signaling without detectable DSBs by neutral comet assay. Additionally, ProKAS biosensor analyses show that the branch of ATM signaling regulated by PPM1D is selectively induced during replication stress recovery, while other branches remain unchanged. Although the precise DNA structures activating ATM at stalled forks remain unclear, we favor the model that ATM senses unprocessed DNA ends at reversed forks. Nevertheless, given previous reports of ATM activation in response to altered chromatin states or oxidative stress (*67*, *68*), we cannot exclude the possibility that chromatin remodeling or oxidative stress during replication stress recovery also contributes to ATM activation.

Another outstanding question is whether ATM signaling at stalled forks plays beneficial roles in maintaining genome stability or supporting replication.One possibility is that early ATM-mediated 53BP1 recruitment to stalled forks, and the consequent suppression of RAD51 loading, allows nucleases such as MRE11 and DNA2 to perform limited resection during recovery from replication stress. This limited ssDNA production is needed for subsequent HR-mediated fork restart.Therefore, PPM1D is needed later in the recovery process to attenuate ATM signaling, reduce 53BP1 engagement and increase RAD51 loading, facilitating the transition from fork processing to HR-mediated fork restart. Importantly, the ability of 53BP1 to antagonize RAD51 loading, a role for 53BP1 also recently demonstrated by others (*63*), may prevent inappropriate or premature recombination events that could cause chromosomal rearrangements. Thus, by orchestrating these dynamic regulatory steps, the ATM–PPM1D axis could ensure a timely, error-free, and balanced coordination of fork protection, processing, and

325 HR-mediated restart. Future investigations will be required to define the spatio-temporal
326 regulation of PPM1D and ATM action at replication forks.

327

328 Alternatively, ATM activation at stalled forks may largely reflect an unintended response to
329 replication intermediates resembling DSBs, such as the DNA end of a regressed fork arm. In
330 this scenario, unchecked ATM signaling may represent a maladaptive response, with PPM1D
331 acting as a safeguard to dampen inappropriate ATM signaling and enable proper fork restart
332 and recovery from replication stress. In the future, it will be important to better characterize the
333 impact of PPM1D and ATM inhibition on the accumulation of replication stress-induced genomic
334 instabilities, such as chromosomal aberrations. Detection of HR-driven chromosomal
335 rearrangements upon ATM inhibition would point to an important role for ATM signaling in
336 promoting HR quality control during replication stress responses. Moreover, delayed RAD51
337 loading and impaired HR-mediated fork restart in the absence of PPM1D may lead to increased
338 utilization of error-prone pathways, such as non-homologous end joining (NHEJ) or
339 microhomology-mediated end joining (MMEJ), resulting in elevated frequencies of chromosomal
340 translocations and radial chromosomes, which can be revealed by metaphase spread analysis.

341

342 These insights have important implications for cancer biology. PPM1D is frequently
343 overexpressed or mutated in cancers, often leading to elevated phosphatase activity. Such
344 dysregulation may enhance cancer cell survival under endogenous or therapy-induced
345 replication stress by facilitating fork restart and recovery (*59*). Pharmacological targeting of
346 PPM1D could synergize with therapies that impair fork remodeling or HR, offering potential
347 strategies to selectively eliminate tumor cells with high levels of replication stress. Going
348 forward, it will be important to assess the generality of PPM1D's role in fork restart across

349 different cell types and biological contexts. Of note, the cell lines used in this study, such as
350 U2OS and HCT116, carry hyper-stabilized forms of PPM1D. It is possible that the dependency
351 on PPM1D varies with the level of ATM signaling, with cells exhibiting higher ATM activity
352 relying more heavily on PPM1D for efficient fork restart, thus exerting selective pressure for
353 mutations that stabilize or increase PPM1D expression.

354

355 In conclusion, this study defines a function for the ATM–PPM1D signaling axis in regulating
356 replication fork restart. By limiting ATM activity at stalled forks, PPM1D enables RAD51
357 recruitment and HR-mediated fork restart and recovery from replication stress. These findings
358 underscore the importance of dynamic phosphorylation control at replication forks and establish
359 PPM1D as a central player in replication stress response pathways with broad relevance to
360 cancer biology and therapeutic intervention.

361

362

363 # METHODS

364

365 **Cell lines and cell culture**

366 All cells were maintained at 37 °C with 5% CO_2 in a humidified incubator and cultured in
367 Dulbecco's Modified Eagle's Medium (DMEM) supplemented with 10% bovine calf serum
368 (BCS), 1% non-essential amino acids, 100 U/mL penicillin, and 100 µg/mL streptomycin. U2OS
369 and HCT116 cells were obtained from the American Type Culture Collection (ATCC). Parental
370 U2OS and U2OS-PPM1D-KO cells were kindly provided by Macurek lab. Parental U2OS and
371 U2OS-SMARCAL1-KO cells were kindly provided by Vindigni lab. Parental U2OS and U2OS-
372 53BP1-KO cells were kindly provided by Durocher lab. All cell lines were regularly tested for
373 mycoplasma contamination using the Universal Mycoplasma Detection Kit (ATCC).

374

375 **Drugs and reagents**

376 Hydroxyurea (HU, Sigma-Aldrich, #H8627), PPM1D inhibitor (GSK2830371, Sigma-Aldrich,
377 #SML1048), CDC7 inhibitor (XL413, Selleck Chemicals, #S7547), DNA2 inhibitor (C5, MCE,
378 #HY-128729), MRE11 inhibitor (Mirin, Selleck Chemicals, #S8096), ATM inhibitor (AZD0156,
379 MedChemExpress, #HY-100016), ATR inhibitor (AZD6738, MedChemExpress, #HY-19323),
380 and RAD51 inhibitor (B02, Selleck Chemicals, #S8434) were used as indicated in the
381 experiments. Sodium L-ascorbate (Sigma-Aldrich, #A7631) and azide-fluor 488 (Sigma-Aldrich,
382 #760765) were used for the EdU incorporation assay. Dharmacon siGENOME non-targeting
383 control siRNA (siCTL, Horizon Discovery, #D-001210-02-05) and siGENOME human PPM1D
384 (siPPM1D, Horizon Discovery, #D-004554-01-0002) were used for siRNA transfection. 5-
385 Bromo-2'-deoxyuridine (BrdU, Sigma-Aldrich, #10280879001), 5-Iodo-2'-deoxyuridine (IdU,
386 Sigma-Aldrich, #I7125), and 5-Chloro-2'-deoxyuridine (CldU, Sigma-Aldrich, #C6891) were used
387 for DNA fiber and combing assays. 2-morpholinoethanesulfonic acid (MES, GoldBio,

388 #M095250), N-lauroylsarcosine sodium salt (Sarkoysl, Sigma-Aldrich, #L5125), and ß-agarase
389 (NEB #M0392L) were used for DNA combing assay. Propidium Iodide (PI, Thermo Fisher
390 Scientific, #P3566) and antifade mounting media with DAPI (Vectashield, #H-1200-10) were
391 used for flow cytometry and imaging experiments as specified.
392
393 **Antibodies**
394 Primary antibodies include: β-actin (Proteintech, #66009-1-Ig), β-tubulin (Proteintech, #66240-1-
395 Ig), Histone H4 (Bethyl Laboratories, #A300-647A), KAP1-pS824 (Bethyl Laboratories, #304-
396 146A), Gamma-H2AX (Bethyl Laboratories, #A300-081A), RPA32 (Bethyl Laboratories, #A300-
397 244A), PCNA (Santa Cruz Biotechnology, #sc-56), CHK1-pS345 (133D3, Cell Signaling
398 Technology, #2348), PPM1D/WIP1 (Santa Cruz Biotechnology, #sc-376257), ATM-pS1981
399 (Cell Signaling Technology, #4526), 53BP1 (Cell Signaling Technology #4937), RAD51
400 (Millipore Sigma, #PC130), Rat anti-BrdU (BU1/75 (ICR1) (Abcam, #6326), Mouse anti-BrdU
401 (B44) (BD Biosciences, #347580). Secondary antibodies include: HRP-conjugated goat anti-
402 mouse IgG (Invitrogen #31430), HRP-conjugated donkey anti-rabbit IgG (Cytiva, #NA934V),
403 Alex Fluor 594 goat anti-mouse IgG (H+L) (Invitrogen, #A11005), Alexa Fluor 555 F(ab')2-Goat
404 anti-rabbit IgG (H+L) (Invitrogen, #A21430), Alexa Fluor 488 goat anti-rabbit IgG (H+L)
405 (Invitrogen, #A11008), Alexa Fluor 488 goat anti-mouse IgG (H+L) (Invitrogen, #A11001).
406
407 **Immunofluorescence**
408 For immunofluorescence experiments, cells (25,000 per well) were seeded onto coverslips in
409 12-well plates. The following day, cells were treated as indicated. Cells were then washed twice
410 with 1 mL ice-cold 1x PBS. Cells were pre-extracted with ice-cold buffer (25 mM HEPES, pH
411 7.5, 50 mM NaCl, 1 mM EDTA, 3 mM $MgCl_2$, 300 mM sucrose, 0.5% Triton X-100) for 5
412 minutes, followed by a PBS wash. Fixation was performed with 4% paraformaldehyde in PBS
413 for 10 minutes at room temperature (RT), followed by three 5-minute washes in PBS. Cells were

414 permeabilized with 0.25% Triton X-100 in PBS for 5 minutes and washed three times in PBS.
415 Cells were blocked with 5% BSA in 1x PBS for 1 hour at RT. Coverslips were then incubated
416 with primary antibodies (1:300 dilution in 5% BSA) for 1 hour at RT or overnight at 4°C. After
417 three washes with 1x PBS, cells were incubated with fluorophore-conjugated secondary
418 antibodies (1:500 dilution in 5% BSA) for 1 hour at RT in the dark. Following three final PBS
419 washes, coverslips were mounted with DAPI-containing antifade mounting medium, sealed with
420 nail polish, and stored at 4°C. Images were acquired using a Leica DMi8 inverted fluorescence
421 microscope and analyzed using Fiji/ImageJ. Statistical analyses were performed using
422 GraphPad Prism v9.
423
424 **EdU incorporation assay**
425 For the EdU incorporation experiment, U2OS cells (25,000 cells per well) were seeded onto
426 coverslips in 12-well plates. The following day, cells were treated as indicated and then
427 processed until permeabilization as immunofluorescence assay. Then, cells were washed by
428 3% BSA in 1x PBS twice at room temperature (RT). Click reactions were performed with pre-
429 mixed reagents (10 mM Na-L-Ascorbate; 0.1 mM Alexa Fluor Azide; 5 mM $CuSO_4$) for 30
430 minutes at RT. Cells were washed by 3% BSA in 1x PBS twice at RT. Cells were blocked and
431 incubated with primary and secondary antibodies as indicated in the immunofluorescence
432 assay. Following three final 1x PBS washes, coverslips were mounted with a DAPI-containing
433 antifade mounting medium, sealed with nail polish, and stored at 4°C. Images were acquired
434 using a Leica DMi8 inverted fluorescence microscope and analyzed using Fiji/ImageJ. Statistical
435 analyses were performed using GraphPad Prism v9.
436
437 **DNA fiber assay**
438 For DNA fiber experiments to monitor replication fork restart, cells were first labeled with 25 μM
439 CldU for the indicated time, then treated with 4 mM HU for 30 minutes to induce fork stalling.

440 After two washes with prewarmed media, cells were incubated in fresh warm media containing
441 250 μM IdU and 10 μM PPM1D inhibitor, with or without additional inhibitors, for the indicated
442 time. For the fork protection assay, cells were sequentially labeled with 25 μM CldU for 30
443 minutes and 250 μM IdU for 30 minutes, followed by treatment with 2 mM HU and/or 10 μM
444 PPM1Di or 100 nM ATMi for 90 minutes. Following treatment, cells were harvested by
445 trypsinization, washed, and resuspended in 1x PBS. Approximately 1,000 cells were pipetted
446 onto clean glass microscope slides and lysed with DNA fiber lysis buffer (200 mM Tris-HCl at
447 pH 7.4, 50 mM EDTA, 0.5% SDS) for 2 minutes. Slides were immediately tilted at a 15º angle to
448 stretch DNA fibers, air-dried for 5 minutes, and fixed in a 3:1 methanol/acetic acid solution for 10
449 minutes at RT. DNA fibers were denatured in 2.5 M HCl for 1 hour, neutralized with 0.4 M Tris-
450 HCl (pH 7.4) for 5 minutes, and washed three times in 1xPBS for 5 minutes each. Slides were
451 blocked for 1 hour in PBS containing 10% goat serum and 10% BSA. Slides were then
452 incubated with mouse anti-BrdU (BD Biosciences, #347580, 1:50) and rat anti-BrdU (Abcam,
453 #ab6326, 1:200) antibodies in PBS with 3% BSA for 1 hour at 37 °C in a humidified chamber.
454 After three 5-min PBS washes, slides were incubated with Alexa Fluor 488-conjugated anti-
455 mouse and Alexa Fluor 594-conjugated anti-rat secondary antibodies (1:500) for 1 hour at RT.
456 Slides were further washed three times in PBS, mounted with Fluoromount-G (Thermo Fisher
457 Scientific), and sealed with nail polish. Images were acquired using a Leica DMi8 inverted
458 fluorescence microscope and analyzed with Fiji/ImageJ software. For fork restart analysis,
459 ongoing forks, bi-directional forks, and terminating forks are classified as restarted forks. The
460 percentages of stalled forks, restarted forks, and newly fired forks were calculated accordingly.
461 Representative images of the different fork types are shown in Fig. S1e. Statistical analyses
462 were performed using GraphPad Prism v9.
463
464 **Western blotting**

465 Cells were lysed in ice-cold modified RIPA buffer (50 mM Tris-HCl, pH 7.5; 150 mM NaCl; 1%
466 Tergitol; 0.25% sodium deoxycholate; 5 mM EDTA) supplemented with complete EDTA-free
467 protease inhibitor cocktail (Roche), 1 mM PMSF, and 5 mM NaF. Lysis was performed for 30
468 minutes at 4 ºC and sonicated. Protein concentration was determined using the Bradford assay
469 (Bio-Rad), and 10-15 µg of total protein was resolved by SDS-PAGE. Proteins were transferred
470 to polyvinylidene difluoride (PVDF) membranes and blocked with 5% non-fat milk in TBST (Tris-
471 buffered saline with 0.05% Tween-20) for 1 hour at RT. Membranes were incubated with
472 primary antibodies overnight at 4 ºC. The following day, membranes were washed three times
473 with TBST and incubated with HRP-conjugated secondary antibodies for 1 hour at RT. After
474 three additional washes with TBST, membranes were developed using Clarity Western ECL
475 substrate (Bio-Rad, #1705060). Chemiluminescent signals were acquired using a ChemiDoc
476 Imaging System (Bio-Rad) and analyzed with ImageLab software (Bio-Rad).
477
478 **Chromatin fractionation**
479 Cells were harvested by trypsinization, washed with PBS, and resuspended in Solution A (10
480 mM HEPES, pH 7.9; 10 mM KCl; 1.5 mM $MgCl_2$; 0.34 M sucrose; 10% glycerol; 0.1% Triton X-
481 100; 1 mM DTT; 10 mM NaF; 1x protease inhibitor cocktail (ThermoFisher, #A32965); 1x
482 PMSF). Cells were incubated on ice for 8 min, then centrifuged at 1,300 x g for 5 minutes at 4
483 ºC. The supernatant was harvested as the cytosolic fraction. The pellet was washed once with
484 solution A, then resuspended in solution B (3 mM EDTA; 0.2 mM EGTA; 1 mM DTT; 1x
485 protease inhibitor cocktail) and incubated on ice for 30 minutes. After centrifugation at 1,700 x g
486 for 5 minutes at 4 ºC, the supernatant was collected as the nucleoplasmic fraction. The
487 remaining pellet was washed once with Solution B and resuspended in the 2x sample buffer for
488 analysis as chromatin fraction. Next, chromatin-associated proteins were analyzed by Western
489 blotting.
490

491 **Clonogenic assay**

492 U2OS cells (800 cells per well) were seeded in 6-well plates and treated with the indicated
493 drugs for 10 days. At the end of the experiment period, cells were washed once with 1x PBS,
494 fixed in 3.7% paraformaldehyde for 10 minutes at RT, and stained with 0.01% crystal violet in 1x
495 PBS solution. Plates were air-dried and scanned, and colony areas were quantified using
496 ImageJ software.

497

498 **Neutral comet assay**

499 Cells were treated as indicated and harvested by trypsinization, followed by a wash with ice-cold
500 1x PBS. Cells were resuspended at a concentration of $1x10^5$/mL and mixed with molten
501 CometAssay® LMAgarose (R&D Systems, #4250-050-02) at a 1:10 (v/v) ratio. A 50 µL aliquot
502 of the mixture was immediately applied onto CometSlide® (R&D Systems, #4250-050-03) and
503 allowed to solidify at 4 ºC for 10 min. Slides were then immersed in lysis solution (R&D
504 Systems, #4250-050-01) for 1 hour at 4 ºC. Following lysis, electrophoresis was carried out
505 under neutral conditions at 1V/cm for 30 minutes at 4 ºC in the dark. Slides were then incubated
506 in DNA precipitation solution (1M ammonium acetate in 82% ethanol) for 30 minutes at RT,
507 followed by a 30-minute incubation in 70% ethanol. Slides were air-dried at 37 °C and stained
508 with SYBR™ Gold (Thermo Fisher Scientific, #S11494). Images were captured at 20x
509 magnification using a Leica DMi8 inverted fluorescence microscope. DNA damage was
510 assessed by measuring the comet tail moment using OpenComet software (v1.3.1).

511

512 **Sample preparation for phosphoproteomic analysis**

513 HCT116 cells were cultured for at least five passages in either “light” or “heavy” SILAC DMEM
514 medium (Thermo Fisher Scientific, #88364) supplemented with 10% dialyzed FBS (Sigma-
515 Aldrich, #F0392), 100 U/mL penicillin, and 100 µg/mL streptomycin (Gibco, #15140-122).
516 Labeling conditions were inverted in biological replicates to filter out phosphopeptides

517 influenced by isotopic bias. After experimental treatments, cells were washed with ice-cold
518 1xPBS and harvested using a cell scraper. Cell pellets were collected by centrifugation at 1,000
519 x g for 5 minutes at 4 °C, washed once in PBS, and stored at -80 °C overnight. Frozen pellets
520 were thawed and resuspended in a hypotonic buffer (20 mM Tris-HCl, pH 7.4; 10 mM NaCl; 3
521 mM $MgCl_2$; 0.5 mM DTT) and incubated on ice for 20 min. Cells were centrifuged at 4,500 x g
522 for 4 minutes at 4 °C and the supernatant was discarded. Pellets were resuspended in lysis
523 buffer (50 mM Tris-HCl, pH 8.0; 0.2% Tergitol; 150 mM NaCl; 5 mM EDTA) supplemented with
524 protease inhibitors (ThermoFisher, #A32965), 1 mM PMSF, and 1x PhosSTOP phosphatase
525 inhibitor cocktail (Roche). Lysis proceeded on ice for 30 min, followed by sonication using a
526 Branson 450 digital sonifier with a 102-C probe (15% amplitude, 3s on/ 2s off pulses) for 50
527 seconds. Lysates were clarified by centrifugation at 45,000 x g for 30 minutes at 4°C.
528 Protein concentrations were determined using the Bradford assay (BioRad). Equal amounts (2
529 mg each) of light- and heavy-labeled lysates were combined. Samples were denatured and
530 reduced with 1% SDS and 5 mM DTT at 65 °C for 10 minutes. Cysteines were alkylated with 25
531 mM iodoacetamide for 15 min in the dark**.** Proteins were precipitated by adding 3 volumes of
532 cold precipitation solution (50% acetone, 49.9% ethanol, 0.1% acetic acid) and incubated on ice
533 for at least 20 minutes. Pellets were recovered by centrifugation at 4,500 x g for 5 minutes at
534 4°C, washed once with 8 M urea solution and deionized water, and centrifuged at 13,000 x g for
535 1 minute. Residual water was carefully removed without disturbing the pellet. Pellets were
536 resuspended in 400 µL of 8 M urea in 100 mM Tris-HCl (pH 8.0), then diluted to 2 M urea by
537 adding 1,200 µL of Tris/NaCl solution (50 mM Tris-HCl, pH 8.0; 150 mM NaCl). Proteins were
538 digested overnight at 37 °C with 4 µg of TPCK-treated trypsin. Peptides were acidified to a final
539 concentration 0.2% trifluoroacetic acid (TFA) and formic acid (FA), and desalted using a 200 mg
540 Sep-Pak C18 cartridge (Waters). Briefly, the C18 column was pre-conditioned with buffer B
541 (80% acetonitrile, 0.1% TFA) followed by buffer A (0.1% TFA). Samples were loaded, washed

542 with buffer C (0.1% acetic acid), and eluted with buffer D (80% acetonitrile, 0.1% acetic acid),
543 then dried in a SpeedVac.
544
545 Phosphopeptides were enriched using the High-Select Fe-NTA phosphopeptide enrichment kit
546 (Thermo Fisher Scientific, #A32992) following the manufacturer's protocol. Eluted
547 phosphopeptides were immediately dried and resuspended in 0.1% TFA, followed by a clean-up
548 using a small-scale C18 spin column (Thermo Fisher Scientific, #89879) packed with C18 slurry.
549 Columns were conditioned with buffer B and A, samples loaded, washed with 3% acetonitrile in
550 buffer A, and eluted with buffer D. Eluted peptides were dried in a SpeedVac.
551
552 Dried phosphopeptides were resuspended in 15 µL LC-grade H_2O, 10 µL 10% FA, and 60 µL
553 HPLC-grade acetonitrile. A total of 80 µL was injected into an UltiMate 3000 system and
554 fractionated by HILIC (hydrophilic interaction liquid chromatography) using a TSKgel Amide-80
555 column (2 mm × 150 mm, 5 µm; Tosoh Bioscience). The following gradient buffers were used:
556 buffer A (90% acetonitrile), buffer B (75%acetonitrile and 0.005% TFA), and buffer C (0.025%
557 TFA). The gradient program was as follows: 100% buffer A (0 min); 94% buffer B/6% buffer C (3
558 min); 65.6% buffer B/34.4% buffer C (30 minutes); and 5% buffer B/95% buffer C (32 - 40
559 minutes). Flow rate: 150 µL/min. Fractions were collected every 30 seconds from minute 5 to
560 minute 24. All fractions were dried, resuspended in 5 µL of 0.1P (1 pmole/µL angiotensin in
561 0.1% TFA), and subjected to LC-MS/MS analysis.
562
563 **ProKAS biosensor sample preparation**
564 Stable U2OS cell lines expressing the ProKAS construct were generated using lentiviral
565 transduction, followed by selection with 1 µg/mL puromycin. Following treatment, cells cultured
566 in 6-well tissue culture plates were lysed using a modified radioimmunoprecipitation assay
567 buffer (mRIPA) buffer supplemented with 0.2% SDS (SDS lysis buffer). After aspirating the

568 culture media, 175 µL of SDS lysis buffer was added to each well. Plates were placed on a hot
569 plate set to 200°C for 10 seconds and immediately removed and agitated to promote the lysis.
570 This heating and agitation step was repeated 2-3 times to ensure complete lysis. Following
571 lysis, 525 µL of mRIPA buffer was added to each well to dilute the final SDS concentration to
572 below 0.1%. Lysates were collected into pre-labeled tubes and sonicated using a Branson 1/8"
573 probe tip sonifier (5 seconds at 12% amplitude) to shear genomic DNA and reduce viscosity.
574 Samples were then centrifuged at 16,000 x g for 3 minutes at 4°C to pellet debris. For affinity
575 purification, 4 µL of ALFA magnetic resin (NanoTag, #N1516) was used per lysate. Resin was
576 equilibrated by resuspending in 1 mL mRIPA buffer, and then distributed evenly to LoBind
577 Eppendorf tubes placed on magnetic racks. Afterwards, the buffer was aspirated, and the
578 lysates were transferred to the tubes containing the immobilized resin. The samples were
579 incubated for 30 minutes at 4°C on a nutating mixer. After incubation, beads were immobilized
580 on magnetic racks and supernatants were aspirated. Beads were washed twice with 500 µL
581 mRIPA buffer and once with 1 mL sterile deionized water, with each wash involving nutation for
582 1 minute at RT. The beads were then immobilized and 80 µL of acidic elution buffer (0.1 M
583 Glycine-HCl, 150 mM NaCl, pH 2.2) was added to each tube. The tubes were agitated for 2
584 minutes at RT to aid in elution of the bait protein. Eluted material was collected into new LoBind
585 Eppendorf tubes. For digestion, each elution was adjusted by adding 20 µL of 1M Tris (pH 8.0),
586 50 µL of 8 M Urea, and 50 µL of 150 mM NaCl-50 mM Tris (pH 8.0) containing 100 ng Trypsin
587 Gold (Promega, #V5280). Samples were incubated at 37 °C on a nutating mixer for 6-18 hours
588 to allow tryptic digestion of immunoprecipitated proteins. Peptide samples were acidified by
589 adding 10 µL of 10% Trifluoroacetic acid (TFA) and 10 µL of 10% Formic Acid. Acidified digests
590 were desalted using 20 mg of C18 resin (Sep-Pak cartridge; Waters, WAT054945) packed into
591 Pierce Micro Spin Columns (ThermoFisher Scientific, #89879). The resin was conditioned with
592 200 µL of 80% acetonitrile (ACN) containing 0.1% TFA, followed by 200 µL 0.1% TFA. Acidified
593 samples were then loaded onto the resin, washed with 350 µL of 0.1% acetic acid, and peptides

594 were eluted into LoBind Eppendorf tubes using 100 µL of 80% ACN containing 0.1% acetic
595 acid. Eluted peptides were then dried in a vacuum concentrator and immediately resuspended
596 in 10 µL of 250 mM HEPES (pH 8.0) for tandem mass tag (TMT) labeling. A 50 µg aliquot of
597 TMTsixplex reagent (ThermoFisher Scientific, #90061) was used to label up to 6 different
598 sample conditions. For each TMT channel, 2 µL of ACN was added to the reagent, followed by
599 the immediate addition of 8 µL of resuspended peptide. Labeling reactions were incubated for
600 60 minutes at RT and quenched by adding 2 µL of 5% hydroxylamine. Subsequently, 25 µL of
601 0.1% TFA was added to each channel. Samples from all channels were then pooled, and an
602 additional 30 µL of 10% TFA was added to the combined sample. The pooled TMT-labeled
603 peptides were desalted again using C18 cleanup as described above. The dried samples were
604 resuspended in LC-grade water prior to MS injection.
605
606 **DNA combing assay**
607 For the DNA combing assay, 200,000 cells were seeded and cultured for 24 hours before
608 labeling. Cells were first labeled with 25 µM CldU for 20 minutes, followed by treatment with 4
609 mM HU for 30 minutes. Cells were washed twice with pre-warmed 1x PBS and incubated in pre-
610 warmed complete medium containing 250 µM IdU, with or without 10 µM PPM1Di for 40
611 minutes. Cells were harvested and resuspended in 1.2 % low-melting-temperature (LMT)
612 agarose (Sigma-Aldrich, #A4018) pre-warmed to 55 ºC and allowed to solidify at 4 ºC for 1 hour.
613 Cell-containing agarose was incubated in ESP solution (200 µL 0.5 M EDTA, pH 8.0; 25 µL 10%
614 Sarkosyl; 50 µL Proteinase K) at 50 ºC for 16 hours. The ESP solution was then discarded, and
615 cells were washed six times with a modified TE buffer (10 mM Tris-HCl, 1 mM EDTA, pH 8.0).
616 Agarose plugs were melted in 1 mL MES buffer (1.22 g MES dissolved in 12.5 mL ddH_2O, pH
617 5.5) at 68 ºC for 20 minutes and further incubated at 42 ºC for 20 minutes. Subsequently, 1.0 µL
618 ß-agarase was added to each sample and digestion was performed at 42 ºC for 12 hours. DNA
619 solutions were transferred into disposable reservoirs (Genomic Vision) and loaded onto the

620 molecular combing system (Genomic Vision). Functionalized microarray coverslips (PolyAn,
621 #10490804) were used for DNA stretching. After combing, coverslips were baked at 65ºC for 2
622 hours and fixed in methanol for 10 minutes at RT. DNA fibers were denatured, blocked,
623 incubated with primary and secondary antibodies as described for the DNA fiber assay. Images
624 were acquired and analyzed as DNA fiber assay. Representative images of different combing
625 conditions are shown in Fig. 1d.
626
627 **siRNA transfection**
628 For siRNA transfection performed in EdU incorporation assay, 10,000 cells per condition were
629 seeded on 6cm plates and incubated at 37 °C until 60%-70% confluent. Then, solution A (3 µL
630 of siRNA (20 pmols) in 250 µL Opti-MEM) and solution B (9 µL of Lipofectamine in 250 µL Opti-
631 MEM) were incubated for 5 minutes at room temperature before mixing. After incubating for 20
632 minutes, the transfection mixture was added drop-wise on cells. Transfection reagents were
633 removed after 6 hours and cells were cultured with complete medium for at least 48 hours,
634 before being treated as indicated in each experiment.
635
636 **MS data acquisition**
637 *Phosphoproteomics*
638 Phosphopeptide fractions were resuspended in 0.1% trifluoroacetic acid and analyzed by liquid
639 chromatography-tandem mass spectrometry (LC-MS/MS) using an UltiMate 3000 HPLC system
640 coupled to a Q-Exactive HF mass spectrometer (Thermo Fisher Scientific). Peptides were
641 separated on a 35 cm in-house packed C18 column (inner diameter of 100 µM) using reversed-
642 phase chromatography. The Q-Exactive HF was operated in data-dependent acquisition (DDA)
643 mode. Full MS scans were acquired in the Orbitrap over a mass-to-charge range of 380-1800
644 *m/z* at a resolution of 60,000. The 20 most abundant precursor ions with charge states of +2,
645 +3, and +4 were selected for MS/MS fragmentation using higher-energy collisional dissociation

646 (HCD) with a normalized collision energy (NCE) of 28. Fragment ion spectra were acquired in
647 the Orbitrap at a resolution of 15,000 with an AGC target of $1x10^5$ and a maximum injection time
648 of 100 ms. Dynamic exclusion was enabled with a 30-second exclusion window to prevent
649 repeated sequencing of previously fragmented ions.
650
651 *ProKAS Sensor*
652 To check the TMT labeling efficiency and retention time of labeled peptides, data-dependent
653 analyses were performed on the Q Exactive HF mass spectrometer using a 70-minute method
654 containing a 60,000 scanning resolution, AGC target of $3x10^6$, maximum inject time of 30 ms,
655 and scan range between 380 and 1800 m/z. The MS2 parameters included a 15,000 resolution,
656 AGC target of $1x10^5$, maximum inject time of 100 ms, isolation window of 2.0 m/z and
657 normalized collision energy (NCE) of 36. Once the mass of target peptides and their
658 phosphorylated forms were identified, parallel reaction monitoring was performed utilizing a 70-
659 minute method with 15,000 resolution, AGC of $2x10^5$, an inject time of 120 ms, and an isolation
660 window of 0.4 m/z. Labeling efficiency was determined to be between 85-90%, and parallel
661 reaction monitoring libraries were determined based on Comet searches to design an inclusion
662 list with peptide masses.
663
664 **Phosphoproteomic data analysis**
665 Raw LC-MS/MS data were analyzed using the Comet search engine. The following search
666 parameters were applied: precursor mass tolerance of ±10 ppm; semi-tryptic digestion; variable
667 modifications of +8.0142 Da (Lysine, heavy SILAC), +10.00827 Da (Arginine, heavy SILAC),
668 +79.966331 Da (phosphorylation of Ser/Thr/Tyr), and +57.021465 (carbamidomethylation of
669 cysteine). Searches were performed against the Uniprot human proteome database (74,304
670 entries). Peptide identification was refined using PeptideProphet, with the following parameters:
671 minimum probability of 0.05, minimum peptide length of 7 residues, accurate mass binning,

672 charge states restriction to +2, +3, and +4, and phospho-site scoring enabled ("use Phospho-
673 information"). Peptide quantification was performed using Xpress, with a mass tolerance of
674 0.005 Da, requiring a minimum of one point for quantitation and one isotopic peak per peptide.
675 Phosphosite localization confidence was determined using PTMProphet. In-house R-scripts
676 were used to further process the data, including: grouping adjacent phosphorylatable residues
677 into phosphosite clusters when exact localization could not be determined; calculating the
678 average and median Xpress ratio for each peptide; computing statistical significance using the
679 Mann-Whitney U test.
680
681 **ProKAS Data Analysis with Skyline**
682 To construct the spectral libraries utilized for ProKAS parallel reaction monitoring, raw MS/MS
683 data generated from the DDA runs were searched on the Comet search engine to obtain
684 peptide masses. The search was conducted using the following parameters: semi-tryptic
685 peptide identification, mass tolerance within 15 ppm, variable modifications for STY
686 phosphorylation (79.966331 Da). The search was performed against the Uniprot human
687 proteome database in addition to ProKAS peptide sequences, as well as the TMT condition.
688 PTMprophet was utilized to determine phosphorylation site localization, search results were
689 imported into Skyline, containing masses of the unphosphorylated and phosphorylated forms of
690 the target ProKAS peptides. Once a library was generated, PRM data was imported into Skyline
691 for analysis by conversion to mzXML format using msConvert. Transitions were verified
692 manually before generating a transitions report from Skyline containing the Protein, Peptide
693 Modified Sequence, Replicate, Precursor Mz, Precursor Charge, Product Mz, Fragment Ion,
694 Retention Time, and Area. Data in these reports were processed for each TMT fragment ion in
695 each replicate by normalization of phosphorylated peptide ratios to their unphosphorylated
696 counterparts. Then, the normalized ratios in each condition were compared against the
697 normalized ratios in the untreated condition to calculate changes in phosphorylation levels for

698 each peptide. Each condition was run in three replicates and error bars in associated figures
699 reflect the standard deviation of the replicates in each condition.
700
701 **Statistical analysis**
702 Statistical analyses were performed using GraphPad Prism. When comparing three or more
703 groups, statistical significance was assessed using one-way ANOVA. For comparisons between
704 two groups, a two-tailed unpaired Student's *t*-test was used. Exact *p*-values, statistical tests, and
705 replicate numbers are detailed in the corresponding figure legends.
706
707 **Data Availability**
708 Mass spectrometry data generated for this study are available through PRIDE, wherein
709 phosphoproteomics data can be found under PXD identifier PXD045462
710 (https://www.ebi.ac.uk/pride/)(*69*).
711

712 ## ACKNOWLEDGEMENTS

713 We thank Libor Macurek for providing U2OS WT and PPM1D-KO cells, Daniel Durocher for
714 providing U2OS WT and 53BP1-KO cells, and Alessandro Vindigni for providing U2OS WT and
715 SMARCAL1-KO cells. We acknowledge the Weill Institute for providing access to the ChemiDoc
716 Imaging system used in this study. We thank Catalina Pereira and Munisha Mujingjiang for
717 providing supplies and technical support to perform DNA combing experiments. We thank
718 Beatriz Almeida for technical assistance and all members of the Smolka lab for helpful
719 discussions and technical support. M.B.S. was supported by NIH grant R35-GM563209. Y.W.
720 was supported by a postdoctoral fellowship from the Fleming Research Foundation.

721 ## AUTHOR CONTRIBUTIONS

722 JB and MBS led the conceptualization of the main study, defining the problem statement and
723 research objectives. YC, YW, and MBS contributed to the conceptualization and refinement of
724 the final study design. JB performed and analyzed immunofluorescence, western blot,
725 chromatin fractionation, comet assays, clonogenic assays, and DNA fiber assays for the initial
726 study. YC performed and analyzed the final experiments for all immunofluorescence, EdU
727 incorporation, western blot, siRNA transfection, and DNA combing assays. YW conducted and
728 analyzed the final experiments for BrdU incorporation, neutral comet assays, and DNA fiber
729 assays. YW and TCH jointly performed and analyzed the clonogenic survival assays. JB and
730 VMF carried out and analyzed the phosphoproteomic experiments. KJ performed and analyzed
731 the ProKAS experiments. EÇ contributed to DNA fiber data analysis for the pilot study. JB, YC,
732 and YW prepared the data visualizations. MBS and JB wrote the initial version of the
733 manuscript, with YC and YW contributing to the final version. YC, YW, KJ, and MBS reviewed
734 and edited the manuscript. MBS secured funding and supervised the project. All authors
735 contributed to and approved the final version of the manuscript.

DECLARATION OF INTERESTS

The authors declare no conflicts of interest.

740 # REFERENCES

741 1. M. K. Zeman, K. A. Cimprich, Causes and consequences of replication stress. *Nat. Cell*
742 *Biol.* **16**, 2–9 (2014).

743 2. S. Saxena, L. Zou, Hallmarks of DNA replication stress. *Mol. Cell* **82**, 2298–2314 (2022).

744 3. P. Pasero, A. Vindigni, Nucleases acting at stalled forks: How to reboot the replication
745 program with a few shortcuts. *Annu. Rev. Genet.* **51**, 477–499 (2017).

746 4. E. A. Nam, D. Cortez, ATR signalling: more than meeting at the fork. *Biochem. J* **436**, 527–
747 536 (2011).

748 5. L. I. Toledo, M. Altmeyer, M.-B. Rask, C. Lukas, D. H. Larsen, L. K. Povlsen, S. Bekker-
749 Jensen, N. Mailand, J. Bartek, J. Lukas, ATR prohibits replication catastrophe by
750 preventing global exhaustion of RPA. *Cell* **155**, 1088–1103 (2013).

751 6. A. P. Bertolin, B. Canal, M. Yekezare, J. Zeng, R. Instrell, M. Howell, J. F. X. Diffley, The
752 mechanism of checkpoint-dependent DNA replication fork stabilization in human cells,
753 *bioRxiv* (2024). https://doi.org/10.1101/2024.11.01.621514.

754 7. W. Leung, A. Simoneau, S. Saxena, J. Jackson, P. S. Patel, M. Limbu, A. Vindigni, L. Zou,
755 ATR protects ongoing and newly assembled DNA replication forks through distinct
756 mechanisms. *Cell Rep.* **42**, 112792 (2023).

757 8. M. El-Shemerly, D. Hess, A. K. Pyakurel, S. Moselhy, S. Ferrari, ATR-dependent pathways
758 control hEXO1 stability in response to stalled forks. *Nucleic Acids Res.* **36**, 511–519 (2008).

759 9. S. Li, Z. Lavagnino, D. Lemacon, L. Kong, A. Ustione, X. Ng, Y. Zhang, Y. Wang, B. Zheng,
760 H. Piwnica-Worms, A. Vindigni, D. W. Piston, Z. You, Ca2+-Stimulated AMPK-Dependent
761 Phosphorylation of Exo1 Protects Stressed Replication Forks from Aberrant Resection.
762 *Mol. Cell* **74**, 1123–1137.e6 (2019).

763 10. M. Berti, D. Cortez, M. Lopes, The plasticity of DNA replication forks in response to
764 clinically relevant genotoxic stress. *Nat. Rev. Mol. Cell Biol.* **21**, 633–651 (2020).

765 11. A. Quinet, D. Lemaçon, A. Vindigni, Replication Fork Reversal: Players and Guardians.
766 *Mol. Cell* **68**, 830–833 (2017).

767 12. M. B. Adolph, D. Cortez, Mechanisms and regulation of replication fork reversal. *DNA*
768 *Repair* **141**, 103731 (2024).

769 13. K. Mutreja, J. Krietsch, J. Hess, S. Ursich, M. Berti, F. K. Roessler, R. Zellweger, M. Patra,
770 G. Gasser, M. Lopes, ATR-Mediated Global Fork Slowing and Reversal Assist Fork
771 Traverse and Prevent Chromosomal Breakage at DNA Interstrand Cross-Links. *Cell Rep.*
772 **24**, 2629–2642.e5 (2018).

773 14. D. Dibitetto, S. Marshall, A. Sanchi, M. Liptay, J. Badar, M. Lopes, S. Rottenberg, M. B.
774 Smolka, DNA-PKcs promotes fork reversal and chemoresistance. *Mol. Cell* **82**, 3932–
775 3942.e6 (2022).

776 15. E. C. Minca, D. Kowalski, Replication fork stalling by bulky DNA damage: localization at
777 active origins and checkpoint modulation. *Nucleic Acids Res.* **39**, 2610–2623 (2011).

778 16. D. V. Bugreev, R. M. Brosh Jr, A. V. Mazin, RECQ1 possesses DNA branch migration
779 activity. *J. Biol. Chem.* **283**, 20231–20242 (2008).

780 17. S. Thangavel, M. Berti, M. Levikova, C. Pinto, S. Gomathinayagam, M. Vujanovic, R.
781 Zellweger, H. Moore, E. H. Lee, E. A. Hendrickson, P. Cejka, S. Stewart, M. Lopes, A.
782 Vindigni, DNA2 drives processing and restart of reversed replication forks in human cells. *J.*
783 *Cell Biol.* **208**, 545–562 (2015).

784 18. L. Costantino, S. K. Sotiriou, J. K. Rantala, S. Magin, E. Mladenov, T. Helleday, J. E.
785 Haber, G. Iliakis, O. P. Kallioniemi, T. D. Halazonetis, Break-induced replication repair of
786 damaged forks induces genomic duplications in human cells. *Science* **343**, 88–91 (2014).

787 19. P. J. Hastings, J. R. Lupski, S. M. Rosenberg, G. Ira, Mechanisms of change in gene copy
788 number. *Nat. Rev. Genet.* **10**, 551–564 (2009).

789 20. M. Ensminger, M. Löbrich, One end to rule them all: Non-homologous end-joining and
790 homologous recombination at DNA double-strand breaks. *Br. J. Radiol.* **93**, 20191054
791 (2020).

792 21. Z. Gyüre, Á. Póti, E. Németh, B. Szikriszt, R. Lózsa, M. Krawczyk, A. L. Richardson, D.
793 Szüts, Spontaneous mutagenesis in human cells is controlled by REV1-Polymerase ζ and
794 PRIMPOL. *Cell Rep.* **42**, 112887 (2023).

795 22. A. Mazouzi, A. Stukalov, A. C. Müller, D. Chen, M. Wiedner, J. Prochazkova, S.-C. Chiang,
796 M. Schuster, F. P. Breitwieser, A. Pichlmair, S. F. El-Khamisy, C. Bock, R. Kralovics, J.
797 Colinge, K. L. Bennett, J. I. Loizou, A Comprehensive Analysis of the Dynamic Response to
798 Aphidicolin-Mediated Replication Stress Uncovers Targets for ATM and ATMIN. *Cell Rep.*
799 **15**, 893–908 (2016).

800 23. N. Kanu, T. Zhang, R. A. Burrell, A. Chakraborty, J. Cronshaw, C. DaCosta, E. Grönroos,
801 H. N. Pemberton, E. Anderton, L. Gonzalez, S. Sabbioneda, H. D. Ulrich, C. Swanton, A.
802 Behrens, RAD18, WRNIP1 and ATMIN promote ATM signalling in response to replication
803 stress. *Oncogene* **35**, 4009–4019 (2016).

804 24. S. A. Wagner, H. Oehler, A. Voigt, D. Dalic, A. Freiwald, H. Serve, P. Beli, ATR inhibition
805 rewires cellular signaling networks induced by replication stress. *Proteomics* **16**, 402–416
806 (2016).

807 25. K. Nakamura, G. Kustatscher, C. Alabert, M. Hödl, I. Forne, M. Völker-Albert, S. Satpathy,
808 T. E. Beyer, N. Mailand, C. Choudhary, A. Imhof, J. Rappsilber, A. Groth, Proteome
809 dynamics at broken replication forks reveal a distinct ATM-directed repair response
810 suppressing DNA double-strand break ubiquitination. *Mol. Cell* **81**, 1084–1099.e6 (2021).

811 26. C. Ribeyre, R. Zellweger, M. Chauvin, N. Bec, C. Larroque, M. Lopes, A. Constantinou,
812 Nascent DNA Proteomics Reveals a Chromatin Remodeler Required for Topoisomerase I
813 Loading at Replication Forks. *Cell Rep.* **15**, 300–309 (2016).

814 27. A. K. Ashley, M. Shrivastav, J. Nie, C. Amerin, K. Troksa, J. G. Glanzer, S. Liu, S. O.
815 Opiyo, D. D. Dimitrova, P. Le, B. Sishc, S. M. Bailey, G. G. Oakley, J. A. Nickoloff, DNA-PK

816 phosphorylation of RPA32 Ser4/Ser8 regulates replication stress checkpoint activation, fork
817 restart, homologous recombination and mitotic catastrophe. *DNA Repair (Amst)* **21**, 131–
818 139 (2014).

819 28. S. Ying, Z. Chen, A. L. Medhurst, J. A. Neal, Z. Bao, O. Mortusewicz, J. McGouran, X.
820 Song, H. Shen, F. C. Hamdy, B. M. Kessler, K. Meek, T. Helleday, DNA-PKcs and PARP1
821 Bind to Unresected Stalled DNA Replication Forks Where They Recruit XRCC1 to Mediate
822 Repair. *Cancer Res* **76**, 1078–1088 (2016).

823 29. M. C. Lanz, D. Dibitetto, M. B. Smolka, DNA damage kinase signaling: checkpoint and
824 repair at 30 years. *EMBO J.* **38**, e101801 (2019).

825 30. D. P. Waterman, J. E. Haber, M. B. Smolka, Checkpoint responses to DNA double-strand
826 breaks. *Annu. Rev. Biochem.* **89**, 103–133 (2020).

827 31. D.-H. Lee, D. Chowdhury, What goes on must come off: phosphatases gate-crash the DNA
828 damage response. *Trends Biochem. Sci.* **36**, 569–577 (2011).

829 32. M. Shimada, M. Nakanishi, Response to DNA damage: why do we need to focus on protein
830 phosphatases? *Front. Oncol.* **3**, 8 (2013).

831 33. A. K. Freeman, A. N. Monteiro, Phosphatases in the cellular response to DNA damage. *Cell*
832 *Commun. Signal.* **8**, 27 (2010).

833 34. X. Lu, B. Nannenga, L. A. Donehower, PPM1D dephosphorylates Chk1 and p53 and
834 abrogates cell cycle checkpoints. *Genes Dev.* **19**, 1162–1174 (2005).

835 35. X. Lu, T.-A. Nguyen, X. Zhang, L. A. Donehower, The Wip1 phosphatase and Mdm2:
836 cracking the "Wip" on p53 stability. *Cell Cycle* **7**, 164–168 (2008).

837 36. S. Shreeram, O. N. Demidov, W. K. Hee, H. Yamaguchi, N. Onishi, C. Kek, O. N. Timofeev,
838 C. Dudgeon, A. J. Fornace, C. W. Anderson, Y. Minami, E. Appella, D. V. Bulavin, Wip1
839 phosphatase modulates ATM-dependent signaling pathways. *Mol. Cell* **23**, 757–764 (2006).

840 37. L. Macůrek, A. Lindqvist, O. Voets, J. Kool, H. R. Vos, R. H. Medema, Wip1 phosphatase is
841 associated with chromatin and dephosphorylates gammaH2AX to promote checkpoint
842 inhibition. *Oncogene* **29**, 2281–2291 (2010).

843 38. X. Lu, T.-A. Nguyen, S.-H. Moon, Y. Darlington, M. Sommer, L. A. Donehower, The type 2C
844 phosphatase Wip1: an oncogenic regulator of tumor suppressor and DNA damage
845 response pathways. *Cancer Metastasis Rev.* **27**, 123–135 (2008).

846 39. J. D. Kahn, P. G. Miller, A. J. Silver, R. S. Sellar, S. Bhatt, C. Gibson, M. McConkey, D.
847 Adams, B. Mar, P. Mertins, S. Fereshetian, K. Krug, H. Zhu, A. Letai, S. A. Carr, J. Doench,
848 S. Jaiswal, B. L. Ebert, PPM1D-truncating mutations confer resistance to chemotherapy
849 and sensitivity to PPM1D inhibition in hematopoietic cells. *Blood* **132**, 1095–1105 (2018).

850 40. P. Kleiblova, I. A. Shaltiel, J. Benada, J. Ševčík, S. Pecháčková, P. Pohlreich, E. E. Voest,
851 P. Dundr, J. Bartek, Z. Kleibl, R. H. Medema, L. Macurek, Gain-of-function mutations of
852 PPM1D/Wip1 impair the p53-dependent G1 checkpoint. *J. Cell Biol.* **201**, 511–521 (2013).

853 41. M. Stoyanov, A. S. Martinikova, K. Matejkova, K. Horackova, P. Zemankova, K. Burdova, Z.
854 Zemanova, P. Kleiblova, Z. Kleibl, L. Macurek, PPM1D activity promotes cellular

855 transformation by preventing senescence and cell death. *Oncogene* **43**, 3081–3093 (2024).

856 42. M. Burocziova, P. Danek, A. Oravetzova, Z. Chalupova, M. Alberich-Jorda, L. Macurek,
857 Ppm1d truncating mutations promote the development of genotoxic stress-induced AML.
858 *Leukemia* **37**, 2209–2220 (2023).

859 43. J. I. Hsu, T. Dayaram, A. Tovy, E. De Braekeleer, M. Jeong, F. Wang, J. Zhang, T. P.
860 Heffernan, S. Gera, J. J. Kovacs, J. R. Marszalek, C. Bristow, Y. Yan, G. Garcia-Manero,
861 H. Kantarjian, G. Vassiliou, P. A. Futreal, L. A. Donehower, K. Takahashi, M. A. Goodell,
862 PPM1D Mutations Drive Clonal Hematopoiesis in Response to Cytotoxic Chemotherapy.
863 *Cell Stem Cell* **23**, 700–713.e6 (2018).

864 44. X. Lu, T.-A. Nguyen, L. A. Donehower, Reversal of the ATM/ATR-mediated DNA damage
865 response by the oncogenic phosphatase PPM1D. *Cell Cycle* **4**, 1060–1064 (2005).

866 45. H. Cha, J. M. Lowe, H. Li, J.-S. Lee, G. I. Belova, D. V. Bulavin, A. J. Fornace Jr, Wip1
867 directly dephosphorylates gamma-H2AX and attenuates the DNA damage response.
868 *Cancer Res.* **70**, 4112–4122 (2010).

869 46. H. Yamaguchi, S. R. Durell, D. K. Chatterjee, C. W. Anderson, E. Appella, The Wip1
870 phosphatase PPM1D dephosphorylates SQ/TQ motifs in checkpoint substrates
871 phosphorylated by PI3K-like kinases. *Biochemistry* **46**, 12594–12603 (2007).

872 47. J. F. Gräf, I. Mikicic, X. Ping, C. Scalera, K. Mayr, L. S. Stelzl, P. Beli, S. A. Wagner,
873 Substrate spectrum of PPM1D in the cellular response to DNA double-strand breaks.
874 *iScience* **25**, 104892 (2022).

875 48. A. G. Gilmartin, T. H. Faitg, M. Richter, A. Groy, M. A. Seefeld, M. G. Darcy, X. Peng, K.
876 Federowicz, J. Yang, S.-Y. Zhang, E. Minthorn, J.-P. Jaworski, M. Schaber, S. Martens, D.
877 E. McNulty, R. H. Sinnamon, H. Zhang, R. B. Kirkpatrick, N. Nevins, G. Cui, B. Pietrak, E.
878 Diaz, A. Jones, M. Brandt, B. Schwartz, D. A. Heerding, R. Kumar, Allosteric Wip1
879 phosphatase inhibition through flap-subdomain interaction. *Nat. Chem. Biol.* **10**, 181–187
880 (2014).

881 49. E. Petermann, M. L. Orta, N. Issaeva, N. Schultz, T. Helleday, Hydroxyurea-stalled
882 replication forks become progressively inactivated and require two different RAD51-
883 mediated pathways for restart and repair. *Mol. Cell* **37**, 492–502 (2010).

884 50. L. Macurek, J. Benada, E. Müllers, V. A. Halim, K. Krejčíková, K. Burdová, S. Pecháčková,
885 Z. Hodný, A. Lindqvist, R. H. Medema, J. Bartek, Downregulation of Wip1 phosphatase
886 modulates the cellular threshold of DNA damage signaling in mitosis. *Cell Cycle* **12**, 251–
887 262 (2013).

888 51. P. Khadka, Z. J. Reitman, S. Lu, G. Buchan, G. Gionet, F. Dubois, D. M. Carvalho, J. Shih,
889 S. Zhang, N. F. Greenwald, T. Zack, O. Shapira, K. Pelton, R. Hartley, H. Bear, Y. Georgis,
890 S. Jarmale, R. Melanson, K. Bonanno, K. Schoolcraft, P. G. Miller, A. L. Condurat, E. M.
891 Gonzalez, K. Qian, E. Morin, J. Langhnoja, L. E. Lupien, V. Rendo, J. Digiacomo, D. Wang,
892 K. Zhou, R. Kumbhani, M. E. Guerra Garcia, C. E. Sinai, S. Becker, R. Schneider, J.
893 Vogelzang, K. Krug, A. Goodale, T. Abid, Z. Kalani, F. Piccioni, R. Beroukhim, N. S.
894 Persky, D. E. Root, A. M. Carcaboso, B. L. Ebert, C. Fuller, O. Babur, M. W. Kieran, C.
895 Jones, H. Keshishian, K. L. Ligon, S. A. Carr, T. N. Phoenix, P. Bandopadhayay, PPM1D
896 mutations are oncogenic drivers of de novo diffuse midline glioma formation. *Nat. Commun.*

897 **13**, 604 (2022).

898 52. J. Yan, X.-P. Yang, Y.-S. Kim, A. M. Jetten, RAP80 responds to DNA damage induced by
899 both ionizing radiation and UV irradiation and is phosphorylated at Ser 205. *Cancer Res* **68**,
900 4269–4276 (2008).

901 53. B. Sobhian, G. Shao, D. R. Lilli, A. C. Culhane, L. A. Moreau, B. Xia, D. M. Livingston, R. A.
902 Greenberg, RAP80 targets BRCA1 to specific ubiquitin structures at DNA damage sites.
903 *Science* **316**, 1198–1202 (2007).

904 54. S.-T. Kim, B. Xu, M. B. Kastan, Involvement of the cohesin protein, Smc1, in Atm-
905 dependent and independent responses to DNA damage. *Genes Dev.* **16**, 560–570 (2002).

906 55. N. Salvador Moreno, J. Liu, K. M. Haas, L. L. Parker, C. Chakraborty, S. J. Kron, K.
907 Hodges, L. D. Miller, C. Langefeld, P. J. Robinson, S. A. Lelièvre, P.-A. Vidi, The nuclear
908 structural protein NuMA is a negative regulator of 53BP1 in DNA double-strand break
909 repair. *Nucleic Acids Res.* **47**, 2703–2715 (2019).

910 56. Y. Ziv, D. Bielopolski, Y. Galanty, C. Lukas, Y. Taya, D. C. Schultz, J. Lukas, S. Bekker-
911 Jensen, J. Bartek, Y. Shiloh, Chromatin relaxation in response to DNA double-strand
912 breaks is modulated by a novel ATM- and KAP-1 dependent pathway. *Nat. Cell Biol.* **8**,
913 870–876 (2006).

914 57. H. Jaiswal, J. Benada, E. Müllers, K. Akopyan, K. Burdova, T. Koolmeister, T. Helleday, R.
915 H. Medema, L. Macurek, A. Lindqvist, ATM/Wip1 activities at chromatin control Plk1 re-
916 activation to determine G2 checkpoint duration. *EMBO J.* **36**, 2161–2176 (2017).

917 58. A. M. Kolinjivadi, V. Sannino, A. de Antoni, H. Técher, G. Baldi, V. Costanzo, Moonlighting
918 at replication forks - a new life for homologous recombination proteins BRCA1, BRCA2 and
919 RAD51. *FEBS Lett.* **591**, 1083–1100 (2017).

920 59. Z. Wang, C. Xu, B. H. Diplas, C. J. Moure, C.-P. J. Chen, L. H. Chen, C. Du, H. Zhu, P. K.
921 Greer, L. Zhang, Y. He, M. S. Waitkus, H. Yan, Targeting mutant PPM1D sensitizes diffuse
922 intrinsic pontine glioma cells to the PARP inhibitor olaparib. *Mol. Cancer Res.* **18**, 968–980
923 (2020).

924 60. K. Burdova, R. Storchova, M. Palek, L. Macurek, WIP1 promotes homologous
925 recombination and modulates sensitivity to PARP inhibitors. *Cells* **8**, 1258 (2019).

926 61. I. Rappold, K. Iwabuchi, T. Date, J. Chen, Tumor suppressor p53 binding protein 1 (53BP1)
927 is involved in DNA damage-signaling pathways. *J. Cell Biol.* **153**, 613–620 (2001).

928 62. L. Feng, N. Li, Y. Li, J. Wang, M. Gao, W. Wang, J. Chen, Cell cycle-dependent inhibition of
929 53BP1 signaling by BRCA1. *Cell Discov.* **1**, 15019 (2015).

930 63. R. Pavani, V. Tripathi, K. B. Vrtis, D. Zong, R. Chari, E. Callen, A. V. Pankajam, G. Zhen,
931 G. Matos-Rodrigues, J. Yang, S. Wu, G. Reginato, W. Wu, P. Cejka, J. C. Walter, A.
932 Nussenzweig, Structure and repair of replication-coupled DNA breaks. *Science* **385**,
933 eado3867 (2024).

934 64. A. N. Blackford, S. P. Jackson, ATM, ATR, and DNA-PK: The Trinity at the heart of the
935 DNA damage response. *Mol. Cell* **66**, 801–817 (2017).

65. W. J. Comstock, M. V. Navarro, D. V. Maybee, Y. Rho, M. Wagner, Y. Wang, M. B. Smolka, Proteomic sensors for quantitative, multiplexed and spatial monitoring of kinase signaling, *bioRxivorg* (2024). https://doi.org/10.1101/2024.12.16.628391.

66. J. L. Johnson, T. M. Yaron, E. M. Huntsman, A. Kerelsky, J. Song, A. Regev, T.-Y. Lin, K. Liberatore, D. M. Cizin, B. M. Cohen, N. Vasan, Y. Ma, K. Krismer, J. T. Robles, B. van de Kooij, A. E. van Vlimmeren, N. Andrée-Busch, N. F. Käufer, M. V. Dorovkov, A. G. Ryazanov, Y. Takagi, E. R. Kastenhuber, M. D. Goncalves, B. D. Hopkins, O. Elemento, D. J. Taatjes, A. Maucuer, A. Yamashita, A. Degterev, M. Uduman, J. Lu, S. D. Landry, B. Zhang, I. Cossentino, R. Linding, J. Blenis, P. V. Hornbeck, B. E. Turk, M. B. Yaffe, L. C. Cantley, An atlas of substrate specificities for the human serine/threonine kinome. *Nature* **613**, 759–766 (2023).

67. C. J. Bakkenist, M. B. Kastan, DNA damage activates ATM through intermolecular autophosphorylation and dimer dissociation. *Nature* **421**, 499–506 (2003).

68. Z. Guo, S. Kozlov, M. F. Lavin, M. D. Person, T. T. Paull, ATM activation by oxidative stress. *Science* **330**, 517–521 (2010).

69. Y. Perez-Riverol, J. Bai, C. Bandla, D. García-Seisdedos, S. Hewapathirana, S. Kamatchinathan, D. J. Kundu, A. Prakash, A. Frericks-Zipper, M. Eisenacher, M. Walzer, S. Wang, A. Brazma, J. A. Vizcaíno, The PRIDE database resources in 2022: a hub for mass spectrometry-based proteomics evidences. *Nucleic Acids Res* **50**, D543–D552 (2022).

957 # FIGURE LEGENDS

958

959 **Figure 1. PPM1D regulates replication fork restart.**

960 (a) EdU incorporation analysis in U2OS cells. Top: experimental scheme illustrating treatment
961 with the PPM1D inhibitor (PPM1Di; GSK2830371; 10 μM). Bottom: dot plot showing EdU
962 intensity in PCNA-positive cells pooled from three independent biological replicates (at least 104
963 cells per condition per replicate). The mean EdU intensity from each replicate is indicated by
964 black dots. *p*-values were determined by one-way ANOVA with Tukey's multiple comparisons
965 test. Error bars represent standard deviation. (b) Representative immunofluorescence images
966 from the EdU incorporation assay shown in (a). Scale bar, 10 μm. (c) EdU incorporation
967 analysis in U2OS wild-type (WT) and PPM1D-knockout (KO) cells. Top: experimental scheme.
968 Bottom: dot plot showing EdU intensity in PCNA-positive cells pooled from three independent
969 biological replicates (at least 83 cells per condition per replicate). The mean EdU intensity from
970 each replicate is indicated by black dots. *p*-values were determined by one-way ANOVA with
971 Tukey's multiple comparisons test. Error bars represent standard deviation. (d) DNA combing
972 assay in U2OS cells. Top: experimental scheme. Bottom left: Representative images of DNA
973 combing assay. Bottom right: bar graph showing the percentages of stalled replication forks in
974 cells treated with or without PPM1Di (10 μM). A minimum of 2,720 fibers were quantified per
975 condition from three independent biological replicates. *p*-values were calculated using Student's
976 t-test. Error bars represent standard deviation. (e) DNA combing assay in U2OS cells
977 transfected with control and PPM1D siRNA (siCTL and si*PPM1D*). Top: experimental scheme.
978 Bottom: bar graph showing the percentages of stalled replication forks in U2OS wild-type (WT)
979 and PPM1D-knockout (KO) cells. A minimum of 1,644 fibers were quantified per condition from
980 two independent biological replicates. *p*-values were calculated using one-way ANOVA with
981 Tukey's multiple comparisons test. Error bars represent standard deviation. (f) Representative

982 immunofluorescence images showing co-staining of PPM1D (red) and EdU (green) detected via
983 anti-PPM1D antibody and click chemistry, respectively. Scale bar, 10 μm. (g) Dot plot showing
984 the PPM1D intensity in EdU-negative and EdU-positive U2OS cells. At least 328 cells were
985 analyzed per condition. *p*-value was calculated using Student's t-test. Error bars represent
986 standard deviation.
987
988 **Figure 2. PPM1D counteracts nucleolytic processing of stalled replication forks.**
989 (a) RPA32 foci analysis in U2OS cells. Top: experimental scheme illustrating treatment with the
990 PPM1D inhibitor (PPM1Di, 10 μM). Bottom: dot plot showing the number of RPA32 foci in
991 PCNA-positive cells pooled from three independent biological replicates (at least 101 cells per
992 condition per replicate). The mean number of RPA32 foci from each replicate is indicated by
993 black dots. *p*-value was calculated using Student's t-test. Error bars represent standard
994 deviation. (b) Representative immunofluorescence images corresponding to (a). Scale bar, 10
995 μm. (c) RPA32 foci analysis in U2OS wild-type (WT) and PPM1D-knockout (KO) cells. Top:
996 experimental scheme. Bottom: dot plot shows the number of RPA32 foci in PCNA-positive cells
997 pooled from three independent biological replicates (at least 101 cells per condition per
998 replicate). The mean number of RPA32 foci from each replicate is indicated by black dots. *p*-
999 value was calculated using Student's t-test. (d) Representative immunofluorescence images
1000 corresponding to (c). Scale bar, 10 μm. (e) Analysis of nascent single-stranded DNA (ssDNA) in
1001 U2OS cells. Top: experimental scheme showing BrdU immunostaining under non-denaturing
1002 conditions following the indicated treatment. Bottom: dot plot shows the number of BrdU foci in
1003 PCNA-positive cells from one representative experiment. Two biological replicates were
1004 performed; results from the second biological replicate are shown in Fig. S2b. *p*-values were
1005 calculated using one-way ANOVA. (f) RPA32 foci analysis in U2OS WT and SMARCAL1-KO
1006 cells. Top: experimental scheme illustrating treatment with the PPM1Di (10 μM). Bottom: dot
1007 plot shows the number of RPA32 foci in PCNA-positive cells pooled from three independent

1008 biological replicates (at least 73 cells per condition per replicate). The mean number of RPA32
1009 foci from each replicate is indicated by black dots. *p*-values were calculated using one-way
1010 ANOVA with Tukey's multiple comparisons test. (g) DNA fiber assay in U2OS WT and
1011 SMARCAL1-KO cells. Top: experimental scheme. Bottom: bar graph shows the percentage of
1012 stalled replication forks in the presence or absence of PPM1Di (10 μM). At least 942 fibers per
1013 condition were quantified across three independent biological replicates. *p*-values were
1014 calculated using one-way ANOVA with Tukey's multiple comparisons test. Error bars represent
1015 standard deviation. (h-i) RPA32 foci analysis in U2OS WT and PPM1D-KO cells treated with or
1016 without MRE11 inhibitor (Mirin; 10 μM) (h) or DNA2 inhibitor (DNA2i; 20 μM) (i), as shown in the
1017 experimental schemes. Dot plots show the number of RPA32 foci in PCNA-positive cells pooled
1018 from three independent biological replicates (at least 97 (h) or 99 (i) cells per condition per
1019 replicate). The mean number of RPA32 foci from each replicate is indicated by black dots. *p*-
1020 values were calculated using one-way ANOVA with Tukey's multiple comparisons test. Error
1021 bars represent standard deviation.
1022
1023 **Figure 3. PPM1D antagonizes ATM signaling during replication stress recovery.**
1024 (a) Scatter plot showing all phosphosites downregulated during replication stress recovery.
1025 Phosphosites from the HU Release/HU Arrest comparison are categorized along the *y*-axis as
1026 either PPM1D-independent (left and center) or PPM1D-dependent (right). (b) Pie chart
1027 summarizing all phosphosites downregulated during replication stress recovery, illustrating the
1028 proportions of PPM1D-independent and PPM1D-dependent sites. (c) Pie chart highlighting the
1029 subset of S/T-Q phosphosites within the PPM1D-independent and PPM1D-dependent groups
1030 shown in (b). (d) Bar graph demonstrating the enrichment of the consensus phospho-motifs
1031 (S/T-Q or S/T-Q-$(D/E)^{2+}$) in cells treated with or without PPM1D inhibitor (PPM1Di). (e)
1032 Immunoblot analysis of U2OS cells treated with hydroxyurea (HU; 4 mM), PPM1Di (10 μM),
1033 and/or ATMi (100 nM) for the indicated times. (f-g) Quantification of relative protein levels of

1034 pKAP1 (f) and pCHK1 (g) based on immunoblot analysis in (e). Bar graphs show normalized
1035 protein expression levels relative to β-actin across three independent biological replicates. The
1036 normalized protein expression level from each replicate is indicated by black dots. *p*-values
1037 were calculated using one-way ANOVA with Tukey's multiple comparisons test. Error bars
1038 represent standard deviation. (h) Phospho-ATM (pATM, S1981) foci analysis in U2OS cells
1039 treated with or without PPM1Di. Dot plot shows the number of pATM foci in PCNA-positive cells
1040 pooled from three independent biological replicates (at least 91 cells per condition per replicate).
1041 The mean number of pATM foci from each replicate is indicated by black dots. *p*-values were
1042 calculated using one-way ANOVA with Tukey's multiple comparisons test. Error bars represent
1043 standard deviation.
1044
1045 **Figure 4. ATM inhibition rescues defects in replication fork processing and restart**
1046 **caused by loss of PPM1D function.**
1047 (a) RPA32 foci analysis in U2OS cells. Top: experimental scheme showing treatment with
1048 PPM1Di and ATM inhibitor (ATMi; AZD0156; 100 nM). Bottom: dot plot shows the number of
1049 RPA32 foci in PCNA-positive cells pooled from three independent biological replicates (at least
1050 93 cells per condition per replicate). The mean number of RPA32 foci from each replicate is
1051 indicated by black dots. *p*-values were calculated using one-way ANOVA with Tukey's multiple
1052 comparisons test. Error bars represent standard deviation. (b) Representative
1053 immunofluorescence images corresponding to the RPA32 foci analysis shown in (a). Scale bar,
1054 10 μm. (c) EdU incorporation analysis in U2OS cells. Top: experimental scheme showing
1055 treatment with PPM1Di and ATMi. Bottom: dot plot shows the EdU intensity in PCNA-positive
1056 cells pooled from three independent biological replicates (at least 95 cells per condition per
1057 replicate). The mean EdU intensity from each replicate is indicated by black dots. *p*-values were
1058 determined by one-way ANOVA with Tukey's multiple comparisons test. Error bars represent
1059 standard deviation. (d) Representative immunofluorescence images from the EdU incorporation

1060 assay shown in (c). Scale bar, 10 μm. (e) DNA fiber assay in U2OS cells. Top: experimental
1061 scheme showing treatment with PPM1Di and ATMi, as indicated. Bottom: bar graph shows the
1062 percentage of stalled replication forks under each treatment condition. A minimum of 2,929
1063 fibers per condition were analyzed from three independent biological replicates. *p*-values were
1064 calculated using one-way ANOVA. Error bars represent standard deviation. (f) DNA protection
1065 assay in U2OS cells. Top: experimental scheme. Bottom: dot plot showing the ratio of IdU/CldU
1066 tract lengths as an indicator of replication fork degradation in one representative experiment. At
1067 least 150 fibers were analyzed per condition. Results from the second biological replicate are
1068 shown in Fig. S3c. *p*-values were calculated using one-way ANOVA. (g) Clonogenic survival
1069 assay of U2OS cells co-treated with ATMi, ATRi, and PPM1Di. Colony area was normalized to
1070 the respective untreated PPM1Di control group for each treatment condition. Data represent
1071 three independent biological replicates. *p*-values were assessed using Student's t-test.
1072
1073 **Figure 5. PPM1D regulates RAD51-mediated replication fork restart.**
1074 (a) RAD51 foci analysis in U2OS cells. Top: experimental scheme. Bottom: dot plot shows the
1075 number of RAD51 foci in PCNA-positive cells pooled from three independent biological
1076 replicates (at least 96 cells per condition per replicate). The mean number of RAD51 foci from
1077 each replicate is indicated by black dots. *p*-value was calculated using Student's t-test. Error
1078 bars represent standard deviation. (b) Representative immunofluorescence images
1079 corresponding to (a). Scale bar, 10 μm. (c) Immunoblot analysis of PPM1D, RAD51, and histone
1080 H4 in chromatin fractions from U2OS cells treated with or without PPM1Di. Ponceau S staining
1081 was used as a loading and total protein normalization control. (d) DNA fiber assay in U2OS
1082 cells. Top: experimental scheme showing treatment with PPM1Di and RAD51 inhibitor (RAD51i;
1083 B02; 20 μM). Bottom: bar graph shows the percentage of stalled replication forks under each
1084 condition. A minimum of 2,959 fibers per condition were quantified from three independent
1085 biological replicates. *p*-values were calculated using one-way ANOVA. Error bars represent

1086 standard deviation. (e) RAD51 foci analysis in U2OS wild-type (WT) and PPM1D-knockout (KO)
1087 cells. Top: experimental scheme. Bottom: dot plot shows the number of RAD51 foci in PCNA-
1088 positive cells pooled from three independent biological replicates (at least 102 cells per
1089 condition per replicate). The mean number of RAD51 foci from each replicate is indicated by
1090 black dots. *p*-values were calculated using one-way ANOVA with Tukey's multiple comparisons
1091 test. Error bars represent standard deviation. (f) 53BP1 foci analysis in U2OS cells. Top:
1092 experimental scheme. Bottom: dot plot shows the number of 53BP1 foci in PCNA-positive cells
1093 pooled from three independent biological replicates (at least 96 cells per condition per replicate).
1094 The mean number of 53BP1 foci from each replicate is indicated by black dots. *p*-values were
1095 calculated using one-way ANOVA with Tukey's multiple comparisons test. Error bars represent
1096 standard deviation. (g) RAD51 foci analysis in U2OS WT and 53BP1-knockout (KO) cells. Top:
1097 experimental scheme. Bottom: dot plot shows the number of RAD51 foci in PCNA-positive cells
1098 pooled from three independent biological replicates (at least 88 cells per condition per replicate).
1099 The mean number of RAD51 foci from each replicate is indicated by black dots. *p*-values were
1100 calculated using one-way ANOVA with Tukey's multiple comparisons test. Error bars represent
1101 standard deviation.
1102
1103 **Figure 6. Increased ATM signaling during fork recovery in cells with impaired PPM1D**
1104 **function is not correlated with an increase in detectable DSB.**
1105 (a) Neutral comet assay in U2OS cells. Top: experimental scheme. Bottom: dot plot shows the
1106 tail moment for each condition. At least 102 cells were quantified per condition. Treatment with 1
1107 μM camptothecin (CPT) for 30 minutes was used as a positive control. *p*-values were calculated
1108 using one-way ANOVA. (b) Immunoblot analysis of phosphorylated KAP1 (pKAP1) in U2OS
1109 cells treated with HU (4 mM) and/or PPM1Di (10 μM) for the indicated durations. The bar graph
1110 at the bottom shows the normalized pKAP1 expression levels relative to β-tubulin from three
1111 independent biological replicates. The normalized pKAP1 expression level from each replicate

1112 is indicated by black dots. *p*-values were calculated using one-way ANOVA with Tukey's
1113 multiple comparisons test. Error bars represent standard deviation. (c) pKAP1 (S824) foci
1114 analysis in U2OS cells. Top: experimental scheme. Bottom: dot plot shows the number of
1115 pKAP1 foci in PCNA-positive cells pooled from three independent biological replicates (at least
1116 125 cells per condition per replicate). The mean number of pKAP1 foci from each replicate is
1117 indicated by black dots. *p*-values were calculated using one-way ANOVA with Tukey's multiple
1118 comparisons test. Error bars represent standard deviation. (d) ProKAS (Proteomic Kinase
1119 Activity Sensor) design. Peptide sequences used in the ATM sensor (PPM1D-untargeted) and
1120 ATM-PPM1D sensor (PPM1D targeted) are shown. (e) Experimental scheme using ProKAS for
1121 detecting ATM and PPM1D activities. (f) Quantification of ATM and PPM1D activity using
1122 ProKAS sensors during replication stress recovery with or without PPM1Di. Bar graphs
1123 represent the normalized ATM activity (left) and PPM1D acitivity (right) relative to untreated
1124 condition from three independent biological replicates. *p*-values were calculated using one-way
1125 ANOVA with Tukey's multiple comparisons test. Error bars represent standard deviation. (g)
1126 Proposed model illustrating how PPM1D promotes replication fork restart and prevents ssDNA
1127 accumulation by counteracting ATM signaling at stalled replication forks.

1128 # SUPPLEMENTAL FIGURE LEGENDS

1129

1130 **Figure S1. PPM1D modulates DNA replication.**

1131 (a) Representative immunofluorescence images from the EdU incorporation assay shown in Fig.
1132 1c. Scale bar, 10 μm. (b) EdU incorporation analysis in U2OS wild-type (WT) and PPM1D-
1133 knockout (KO) cells transfected with control or PPM1D siRNA (siCTL and si*PPM1D*). Top:
1134 experimental scheme. Bottom: dot plot showing EdU intensity in PCNA-positive cells from one
1135 representative experiment. A minimum of 400 cells were quantified per condition from two
1136 independent biological replicates. *p*-values were determined by one-way ANOVA with Tukey's
1137 multiple comparisons test. Error bars represent standard deviation. (c) DNA combing assay in
1138 U2OS cells. Top: experimental scheme. Bottom: bar graph showing the percentages of
1139 restarted replication forks in cells treated with or without PPM1Di (10 μM). A minimum of 2,720
1140 fibers were quantified per condition from three independent biological replicates. *p*-values were
1141 calculated using Student's t-test. Error bars represent standard deviation. (d) DNA combing
1142 assay in U2OS wild-type (WT) and PPM1D-knockout (KO) cells transfected with control or
1143 PPM1D siRNA (siCTL and si*PPM1D*). Top: experimental scheme. Bottom: bar graph showing
1144 the percentages of restarted replication forks. A minimum of 1,644 fibers were quantified per
1145 condition from two independent biological replicates. *p*-values were calculated using one-way
1146 ANOVA with Tukey's multiple comparisons test. Error bars represent standard deviation. (e)
1147 Representative images of different fork types in the DNA fiber assay. (f) DNA fiber assay in
1148 U2OS and HCT116 cells. Top: experimental scheme. Bottom: bar graphs show the percentages
1149 of restarted, stalled and newly fired replication forks in cells treated with or without PPM1Di (10
1150 μM). A minimum of 471 fibers (U2OS) and 641 fibers (HCT116) were quantified per condition
1151 from three independent biological replicates. *p*-values were calculated using Student's t-test.
1152 Error bars represent standard deviation. (g) EdU incorporation analysis in U2OS cells. Top:
1153 experimental scheme illustrating treatment with the PPM1D inhibitor (10 μM) and/or CDC7

1154 inhibitor (CDC7i; XL413; 20 μM). Bottom: dot plot showing EdU intensity in PCNA-positive cells
1155 pooled from three independent biological replicates (at least 73 cells per condition per replicate).
1156 The mean EdU intensity from each replicate is indicated by black dots. *p*-values were
1157 determined by one-way ANOVA with Tukey's multiple comparisons test. Error bars represent
1158 standard deviation.
1159
1160 **Figure S2. PPM1D regulates RPA32 foci accumulation and replication-associated ssDNA**
1161 **formation.**
1162 (a) Representative immunofluorescence images corresponding to Fig. 2e. (b) Analysis of
1163 nascent single-stranded DNA (ssDNA) in U2OS cells using BrdU immunostaining under non-
1164 denaturing conditions, as shown in the treatment scheme. Dot plot shows the number of BrdU
1165 foci in PCNA-positive cells from a second biological replicate. At least 113 PCNA-positive cells
1166 were quantified per condition. *p*-values were calculated using one-way ANOVA. (c) DNA fiber
1167 assay in U2OS WT and SMARCAL1-KO cells. Bar graphs showing the percentage of restarted
1168 (left) or newly fired (right) replication forks in the presence or absence of PPM1D inhibitor
1169 (PPM1Di). At least 942 fibers per condition were quantified per condition across three
1170 independent biological replicates. *p*-values were calculated using one-way ANOVA with Tukey's
1171 multiple comparisons test. Error bars represent standard deviation. A schematic of the fiber
1172 assay condition is shown at the top of the panel.
1173
1174
1175 **Figure S3. ATM inhibition rescues replication fork restart.**
1176
1177 (a) EdU incorporation assay in U2OS cells. Top: experimental schemes showing treatment with
1178 and without HU (4 mM), PPM1Di (Low dose: 3 μM, High dose: 10 μM) and ATMi (100 nM).
1179 Bottom: dot plot shows the EdU intensity in PCNA-positive cells from one representative
1180 experiment (at least 196 cells per condition). *p*-values were determined by one-way ANOVA

with Tukey's multiple comparisons test. Error bars represent standard deviation. (b) DNA fiber assay in U2OS cells treated with or without PPM1Di (10 μM) and ATMi (100 nM). Bar graphs showing the percentage of restarted (left) or newly fired (right) replication forks under each treatment condition across three independent biological replicates. *p*-values were calculated using one-way ANOVA with Tukey's multiple comparisons test. Error bars represent standard deviation. A schematic of the fiber assay condition is shown at the top of the panel. (c) DNA protection assay in U2OS cells treated with or without PPM1Di (10 μM) and ATMi (100 nM), as indicated. Dot plot showing the ratio of IdU/CldU tract lengths as indicator of replication fork degradation from a second biological replicate. At least 144 fibers were analyzed per condition. *p*-values were calculated using one-way ANOVA.

Figure S4. PPM1D regulates RAD51-mediated replication fork restart.

DNA fiber assay in U2OS cells treated with or without PPM1Di (10 μM) and RAD51 inhibitor (RAD51i; B02; 20 μM). Bar graphs showing the percentage of newly fired (left) or restarted (right) replication forks under each treatment condition across three independent biological replicates. *p*-values were calculated using one-way ANOVA with Tukey's multiple comparisons test. Error bars represent standard deviation. A schematic of the fiber assay condition is shown at the top of the panel.

Figure S5. PPM1D inhibition induces phosphorylation of ProKAS sensors in an ATM-dependent manner.

Quantification of ATM and PPM1D activity using ProKAS sensors during replication stress recovery in the presence of PPM1Di (10 μM), with or without ATMi (100 nM). Bar graphs represent the normalized ATM activity (left) and PPM1D acitivity (right) relative to untreated condition from three independent biological replicates. *p*-values were calculated using Student’s t-test. Error bars represent standard deviation.

Figure 1

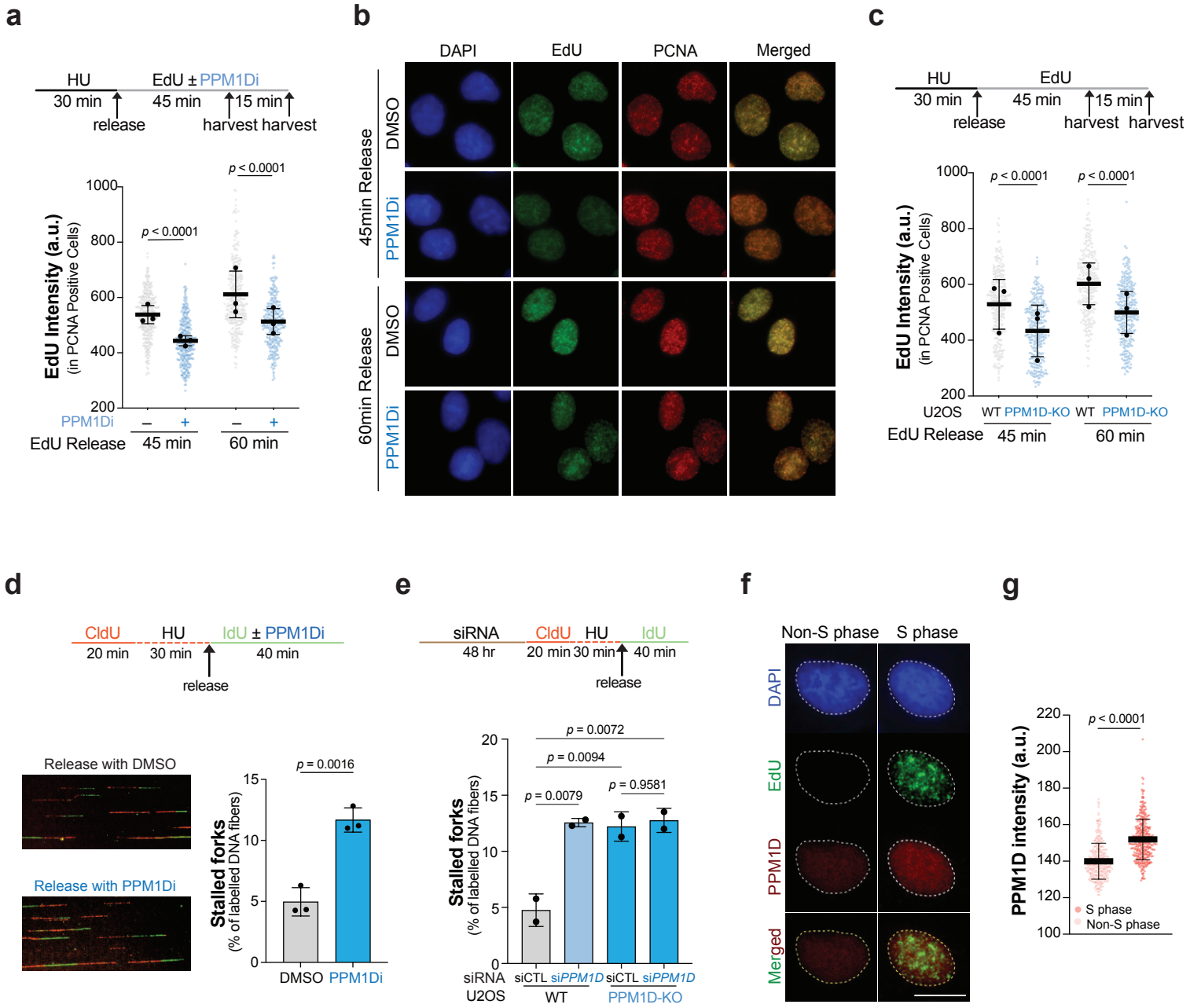
a
HU
EdU ± PPM1Di
30 min
45 min
15 min
release
harvest harvest
p < 0.0001
p < 0.0001
EdU Intensity (a.u.)
(in PCNA Positive Cells)
1000
800
600
400
200
PPM1Di
–
+
–
+
EdU Release
45 min
60 min
b
DAPI
EdU
PCNA
Merged
45min Release
60min Release
DMSO
PPM1Di
DMSO
PPM1Di
c
HU
EdU
30 min
45 min
15 min
release
harvest harvest
p < 0.0001
p < 0.0001
EdU Intensity (a.u.)
(in PCNA Positive Cells)
1000
800
600
400
200
U2OS
WT
PPM1D-KO
WT
PPM1D-KO
EdU Release
45 min
60 min
d
CldU
HU
IdU ± PPM1Di
20 min
30 min
40 min
release
Release with DMSO
Release with PPM1Di
p = 0.0016
Stalled forks
(% of labelled DNA fibers)
15
10
5
0
DMSO
PPM1Di
e
siRNA
CldU
HU
IdU
48 hr
20 min
30 min
40 min
release
p = 0.0072
p = 0.0094
p = 0.0079
p = 0.9581
Stalled forks
(% of labelled DNA fibers)
20
15
10
5
0
siRNA
siCTL
siPPM1D
siCTL
siPPM1D
U2OS
WT
PPM1D-KO
f
Non-S phase
S phase
DAPI
EdU
PPM1D
Merged
g
p < 0.0001
PPM1D intensity (a.u.)
220
200
180
160
140
120
100
S phase
Non-S phase

Figure 2

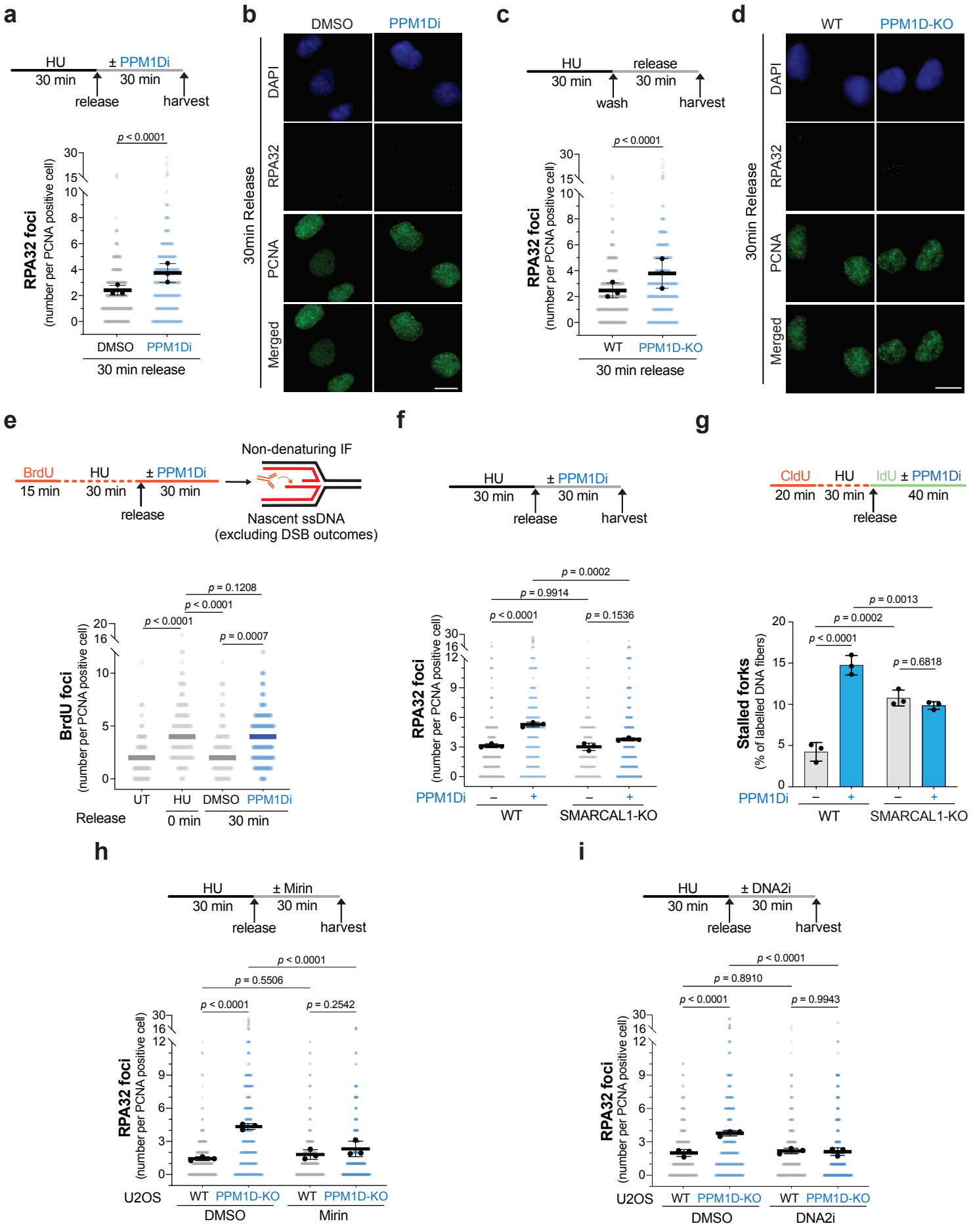
a
HU
30 min
± PPM1Di
30 min
release
harvest
p < 0.0001
RPA32 foci
(number per PCNA positive cell)
DMSO
PPM1Di
30 min release
b
DMSO
PPM1Di
DAPI
RPA32
PCNA
Merged
30min Release
c
HU
30 min
release
30 min
wash
harvest
p < 0.0001
RPA32 foci
(number per PCNA positive cell)
WT
PPM1D-KO
30 min release
d
WT
PPM1D-KO
DAPI
RPA32
PCNA
Merged
30min Release
e
BrdU
15 min
HU
30 min
± PPM1Di
30 min
release
Non-denaturing IF
Nascent ssDNA
(excluding DSB outcomes)
p = 0.1208
p < 0.0001
p < 0.0001
p = 0.0007
BrdU foci
(number per PCNA positive cell)
UT
HU
DMSO
PPM1Di
Release
0 min
30 min
f
HU
30 min
± PPM1Di
30 min
release
harvest
p = 0.0002
p = 0.9914
p < 0.0001
p = 0.1536
RPA32 foci
(number per PCNA positive cell)
PPM1Di
WT
SMARCAL1-KO
g
CldU
20 min
HU
30 min
IdU
± PPM1Di
40 min
release
p = 0.0013
p = 0.0002
p < 0.0001
p = 0.6818
Stalled forks
(% of labelled DNA fibers)
PPM1Di
WT
SMARCAL1-KO
h
HU
30 min
± Mirin
30 min
release
harvest
p < 0.0001
p = 0.5506
p < 0.0001
p = 0.2542
RPA32 foci
(number per PCNA positive cell)
U2OS
WT
PPM1D-KO
DMSO
Mirin
i
HU
30 min
± DNA2i
30 min
release
harvest
p < 0.0001
p = 0.8910
p < 0.0001
p = 0.9943
RPA32 foci
(number per PCNA positive cell)
U2OS
WT
PPM1D-KO
DMSO
DNA2i

Figure 3

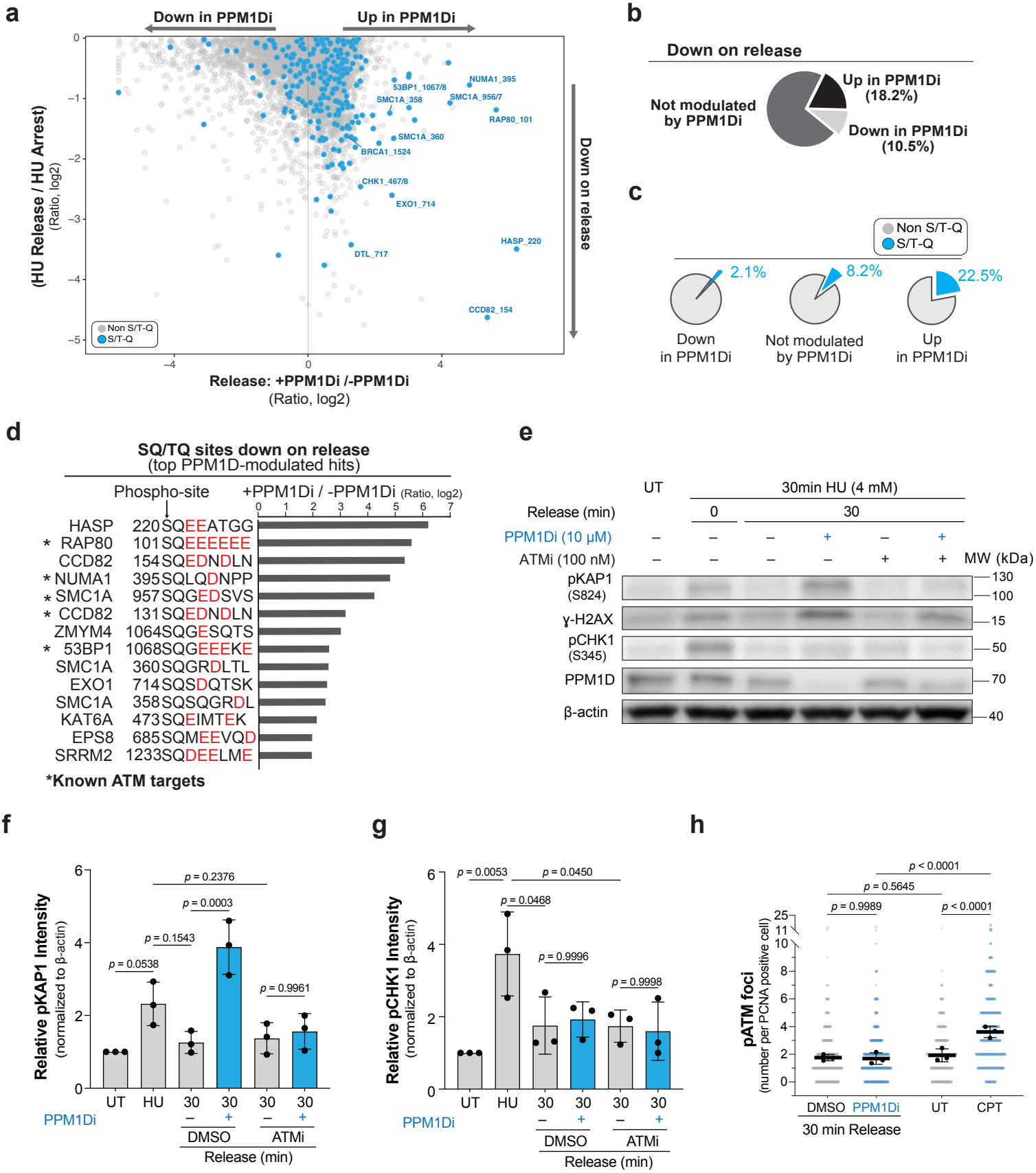
a
Down in PPM1Di
Up in PPM1Di
Down on release
(HU Release / HU Arrest)
(Ratio, log2)
Release: +PPM1Di /-PPM1Di
(Ratio, log2)
Non S/T-Q
S/T-Q
53BP1_1067/8
NUMA1_395
SMC1A_358
SMC1A_956/7
RAP80_101
SMC1A_360
BRCA1_1524
CHK1_467/8
EXO1_714
HASP_220
DTL_717
CCD82_154
b
Down on release
Not modulated by PPM1Di
Up in PPM1Di (18.2%)
Down in PPM1Di (10.5%)
c
Non S/T-Q
S/T-Q
2.1%
8.2%
22.5%
Down in PPM1Di
Not modulated by PPM1Di
Up in PPM1Di
d
SQ/TQ sites down on release
(top PPM1D-modulated hits)
Phospho-site
+PPM1Di / -PPM1Di (Ratio, log2)
HASP 220 SQEEATGG
* RAP80 101 SQEEEEEE
CCD82 154 SQEDNDLN
* NUMA1 395 SQLQDNPP
* SMC1A 957 SQGEDSVS
* CCD82 131 SQEDNDLN
ZMYM4 1064 SQGESQTS
* 53BP1 1068 SQGEEEKE
SMC1A 360 SQGRDLTL
EXO1 714 SQSDQTSK
SMC1A 358 SQSQGRDL
KAT6A 473 SQEIMTEK
EPS8 685 SQMEEVQD
SRRM2 1233 SQDEELME
*Known ATM targets
e
UT
30min HU (4 mM)
Release (min)
0
30
PPM1Di (10 μM)
ATMi (100 nM)
MW (kDa)
pKAP1 (S824)
γ-H2AX
pCHK1 (S345)
PPM1D
β-actin
130
100
15
50
70
40
f
Relative pKAP1 Intensity
(normalized to β-actin)
p = 0.2376
p = 0.0003
p = 0.1543
p = 0.0538
p = 0.9961
UT
HU
PPM1Di
DMSO
ATMi
Release (min)
g
Relative pCHK1 Intensity
(normalized to β-actin)
p = 0.0053
p = 0.0450
p = 0.0468
p = 0.9996
p = 0.9998
h
pATM foci
(number per PCNA positive cell)
p < 0.0001
p = 0.5645
p = 0.9989
p < 0.0001
DMSO
PPM1Di
UT
CPT
30 min Release

Figure 4

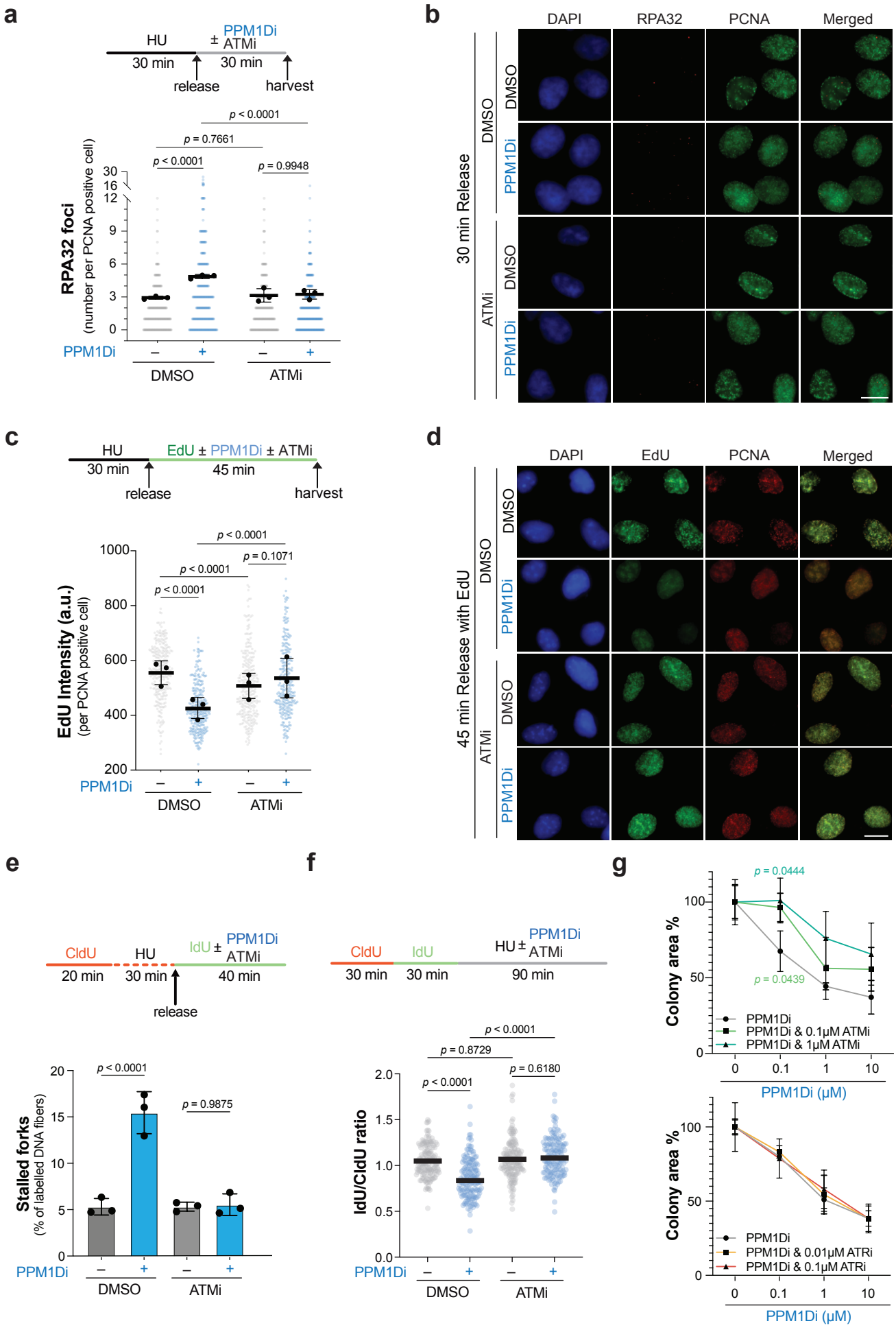
a
HU
30 min
release
± PPM1Di ATMi
30 min
harvest
RPA32 foci
(number per PCNA positive cell)
p < 0.0001
p = 0.7661
p < 0.0001
p = 0.9948
PPM1Di
DMSO
ATMi
b
DAPI
RPA32
PCNA
Merged
30 min Release
DMSO
PPM1Di
ATMi
c
HU
30 min
release
EdU ± PPM1Di ± ATMi
45 min
harvest
EdU Intensity (a.u.)
(per PCNA positive cell)
p < 0.0001
p = 0.1071
d
DAPI
EdU
PCNA
Merged
45 min Release with EdU
e
CldU
20 min
HU
30 min
IdU ± PPM1Di ATMi
40 min
release
Stalled forks
(% of labelled DNA fibers)
p = 0.9875
f
CldU
30 min
IdU
30 min
HU ± PPM1Di ATMi
90 min
IdU/CldU ratio
p = 0.8729
p = 0.6180
g
Colony area %
p = 0.0444
p = 0.0439
PPM1Di
PPM1Di & 0.1μM ATMi
PPM1Di & 1μM ATMi
PPM1Di (μM)
PPM1Di & 0.01μM ATRi
PPM1Di & 0.1μM ATRi

Figure 5

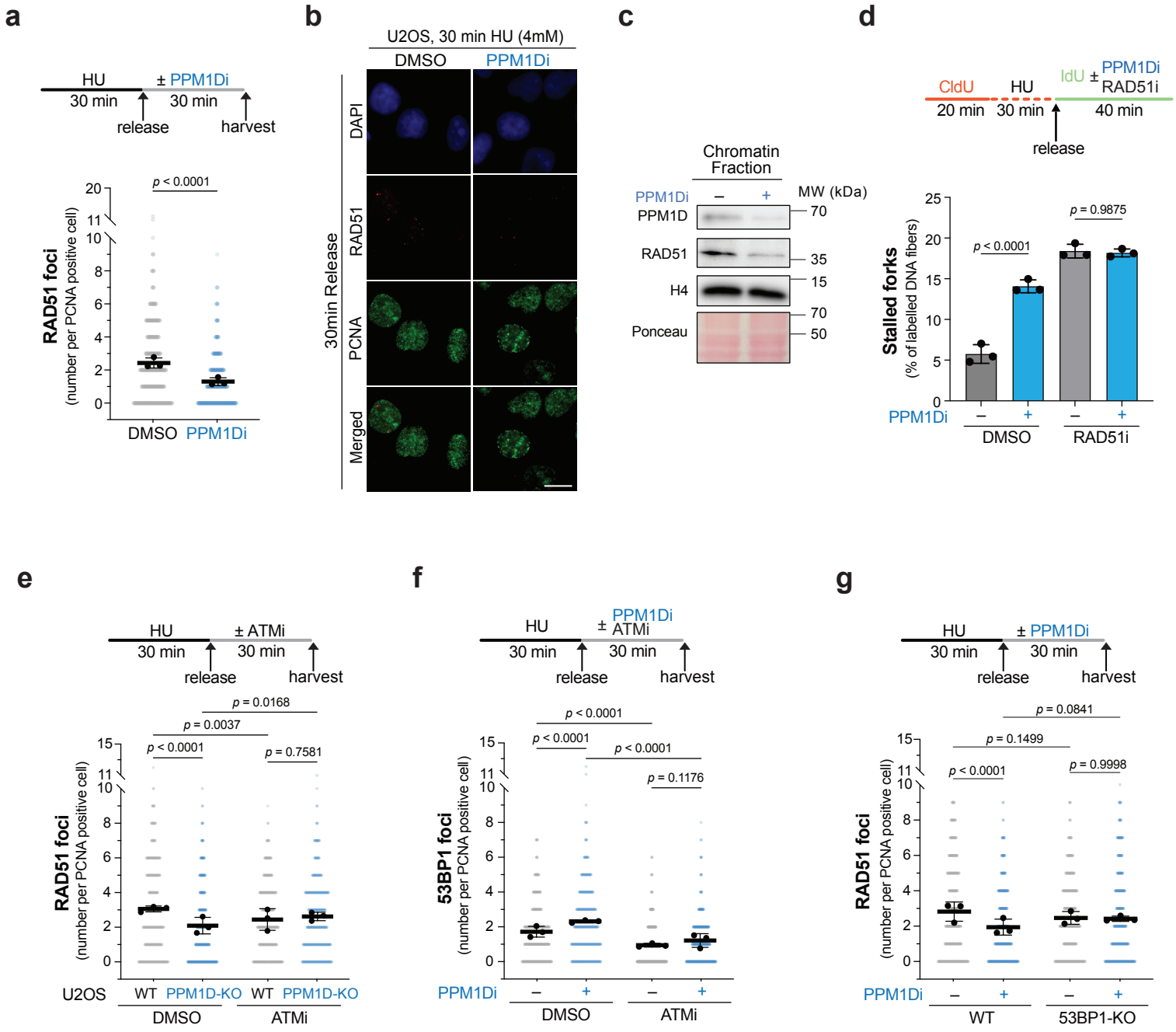
a
HU
30 min
± PPM1Di
30 min
release
harvest
RAD51 foci
(number per PCNA positive cell)
p < 0.0001
DMSO
PPM1Di
b
U2OS, 30 min HU (4mM)
DMSO
PPM1Di
30min Release
DAPI
RAD51
PCNA
Merged
c
Chromatin Fraction
PPM1Di
–
+
MW (kDa)
PPM1D
RAD51
H4
Ponceau
70
35
15
70
50
d
CldU
20 min
HU
30 min
IdU
± PPM1Di
RAD51i
40 min
release
Stalled forks
(% of labelled DNA fibers)
p < 0.0001
p = 0.9875
PPM1Di
DMSO
RAD51i
e
HU
30 min
± ATMi
30 min
release
harvest
RAD51 foci
(number per PCNA positive cell)
p = 0.0168
p = 0.0037
p < 0.0001
p = 0.7581
U2OS
WT
PPM1D-KO
WT
PPM1D-KO
DMSO
ATMi
f
HU
30 min
PPM1Di
± ATMi
30 min
release
harvest
53BP1 foci
(number per PCNA positive cell)
p < 0.0001
p < 0.0001
p < 0.0001
p = 0.1176
PPM1Di
DMSO
ATMi
g
HU
30 min
± PPM1Di
30 min
release
harvest
RAD51 foci
(number per PCNA positive cell)
p = 0.0841
p = 0.1499
p < 0.0001
p = 0.9998
PPM1Di
WT
53BP1-KO

Figure 6

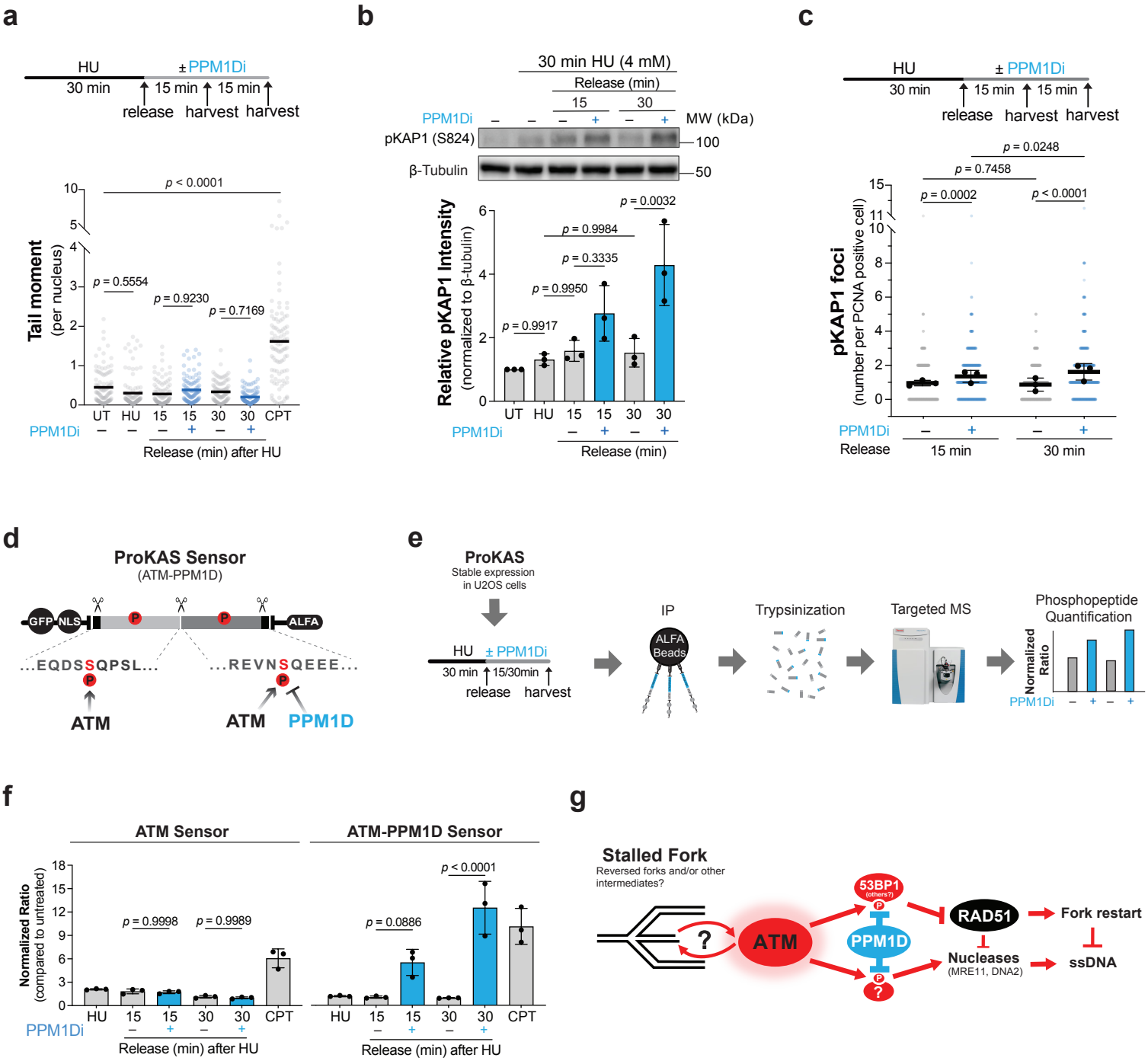
a
HU
± PPM1Di
30 min
15 min
15 min
release
harvest
harvest
Tail moment
(per nucleus)
p < 0.0001
p = 0.5554
p = 0.9230
p = 0.7169
UT HU 15 15 30 30 CPT
PPM1Di
Release (min) after HU
b
30 min HU (4 mM)
Release (min)
15
30
PPM1Di
MW (kDa)
pKAP1 (S824)
β-Tubulin
100
50
Relative pKAP1 Intensity
(normalized to β-tubulin)
p = 0.0032
p = 0.9984
p = 0.3335
p = 0.9950
p = 0.9917
UT HU 15 15 30 30
PPM1Di
Release (min)
c
HU
± PPM1Di
30 min
15 min
15 min
release
harvest
harvest
pKAP1 foci
(number per PCNA positive cell)
p = 0.0248
p = 0.7458
p = 0.0002
p < 0.0001
PPM1Di
Release
15 min
30 min
d
ProKAS Sensor
(ATM-PPM1D)
GFP
NLS
ALFA
...EQDSSQPSL...
...REVNSQEEE...
ATM
ATM
PPM1D
e
ProKAS
Stable expression
in U2OS cells
HU
± PPM1Di
30 min
15/30min
release
harvest
IP
ALFA
Beads
Trypsinization
Targeted MS
Phosphopeptide
Quantification
Normalized
Ratio
PPM1Di
f
ATM Sensor
ATM-PPM1D Sensor
Normalized Ratio
(compared to untreated)
p = 0.9998
p = 0.9989
p = 0.0886
p < 0.0001
HU 15 15 30 30 CPT
PPM1Di
Release (min) after HU
g
Stalled Fork
Reversed forks and/or other
intermediates?
?
ATM
53BP1
(others?)
PPM1D
RAD51
Nucleases
(MRE11, DNA2)
Fork restart
ssDNA

Figure S1

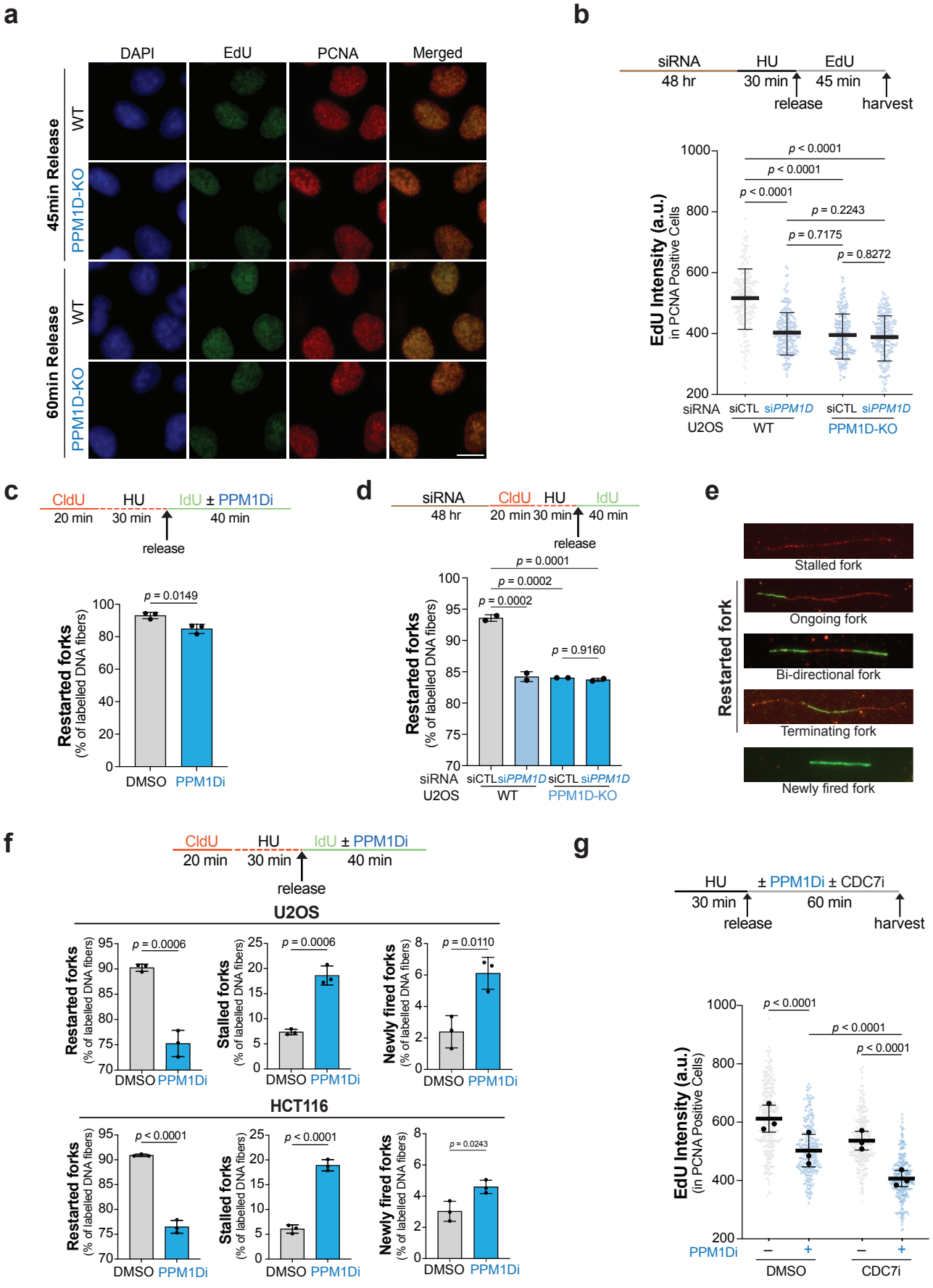
a
DAPI
EdU
PCNA
Merged
45min Release
60min Release
WT
PPM1D-KO
b
siRNA
48 hr
HU
30 min
EdU
45 min
release
harvest
EdU Intensity (a.u.)
in PCNA Positive Cells
p < 0.0001
p < 0.0001
p < 0.0001
p = 0.2243
p = 0.7175
p = 0.8272
siRNA
siCTL
siPPM1D
U2OS
WT
PPM1D-KO
c
CldU
HU
IdU ± PPM1Di
20 min
30 min
40 min
release
Restarted forks
(% of labelled DNA fibers)
p = 0.0149
DMSO
PPM1Di
d
siRNA
48 hr
CldU
HU
IdU
20 min
30 min
40 min
release
p = 0.0001
p = 0.0002
p = 0.0002
p = 0.9160
Restarted forks
(% of labelled DNA fibers)
siRNA
siCTL
siPPM1D
U2OS
WT
PPM1D-KO
e
Restarted fork
Stalled fork
Ongoing fork
Bi-directional fork
Terminating fork
Newly fired fork
f
CldU
HU
IdU ± PPM1Di
20 min
30 min
40 min
release
U2OS
Restarted forks
(% of labelled DNA fibers)
p = 0.0006
Stalled forks
(% of labelled DNA fibers)
p = 0.0006
Newly fired forks
(% of labelled DNA fibers)
p = 0.0110
DMSO
PPM1Di
HCT116
Restarted forks
(% of labelled DNA fibers)
p < 0.0001
Stalled forks
(% of labelled DNA fibers)
p < 0.0001
Newly fired forks
(% of labelled DNA fibers)
p = 0.0243
DMSO
PPM1Di
g
HU
± PPM1Di ± CDC7i
30 min
60 min
release
harvest
EdU Intensity (a.u.)
(in PCNA Positive Cells)
p < 0.0001
p < 0.0001
p < 0.0001
PPM1Di
–
+
DMSO
CDC7i

Figure S2

a

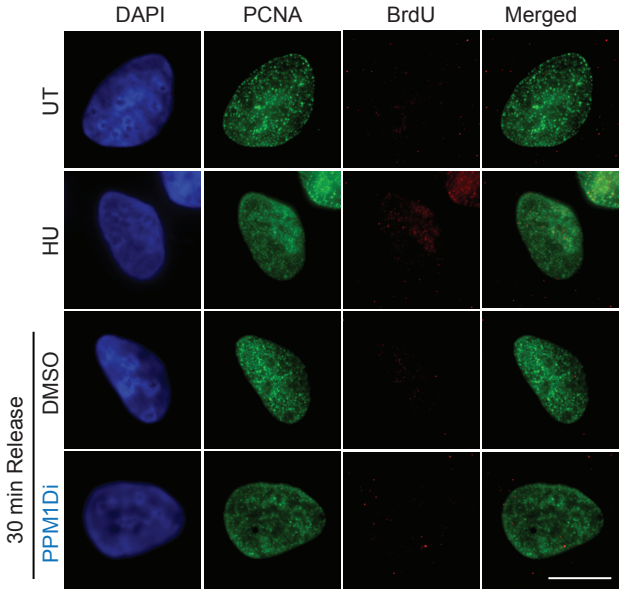

b

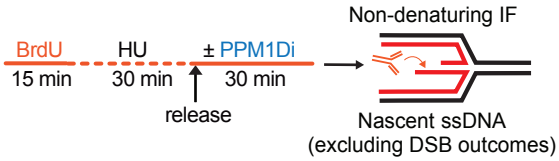

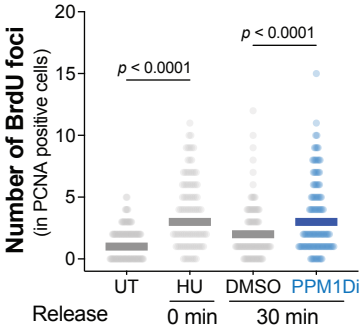

c

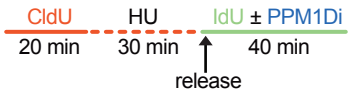

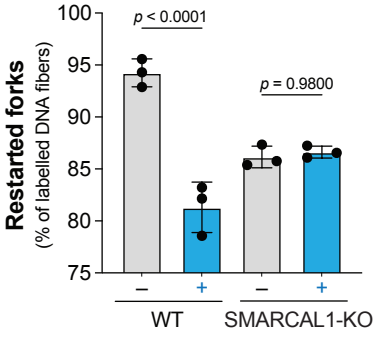

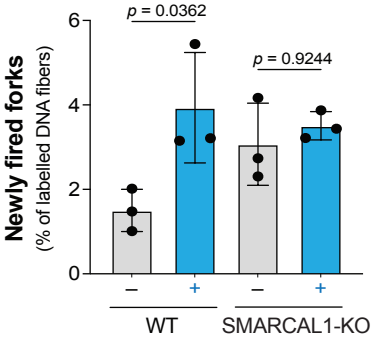

Figure S3

a

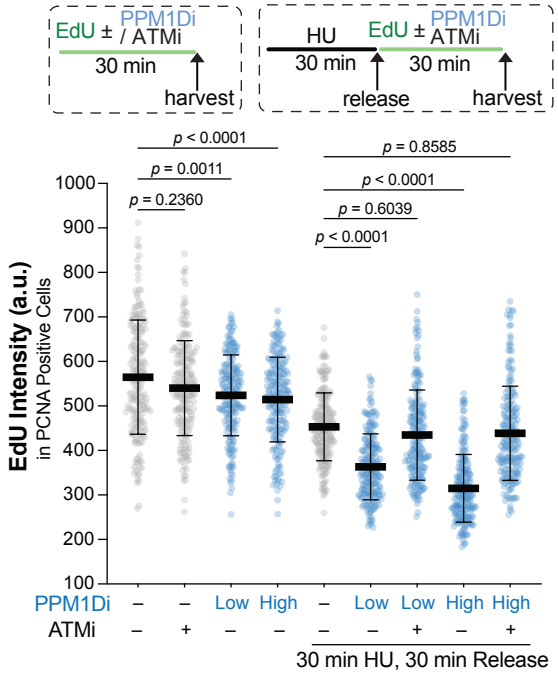

b

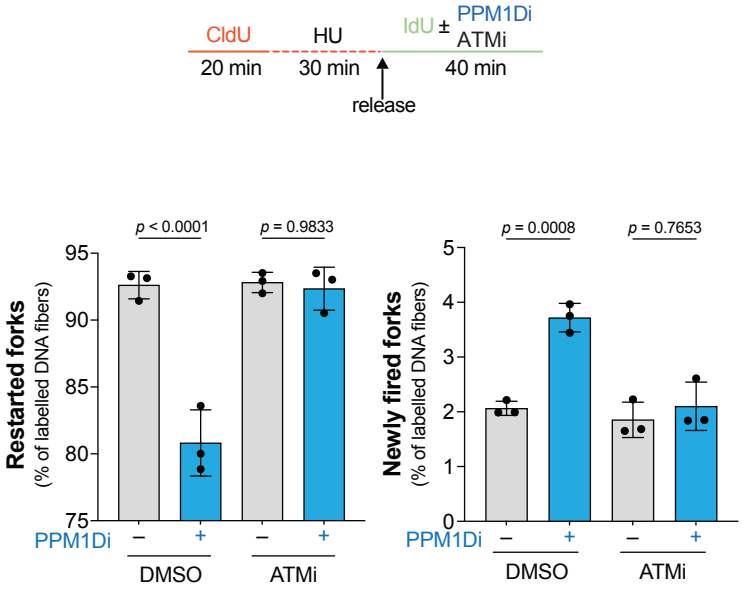

c

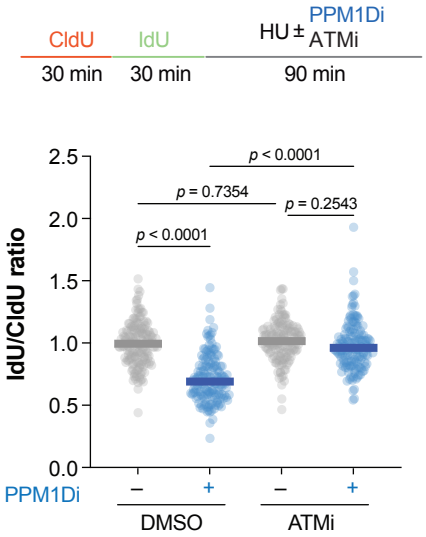

Figure S4

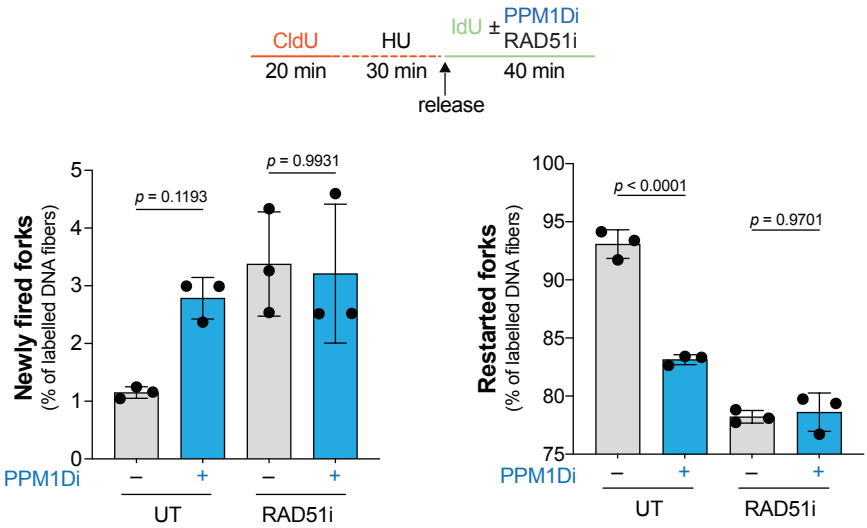
CldU
HU
IdU ±
PPM1Di
RAD51i
20 min
30 min
40 min
release
Newly fired forks
(% of labelled DNA fibers)
p = 0.1193
p = 0.9931
PPM1Di
UT
RAD51i
Restarted forks
(% of labelled DNA fibers)
p < 0.0001
p = 0.9701
PPM1Di
UT
RAD51i

Figure S5

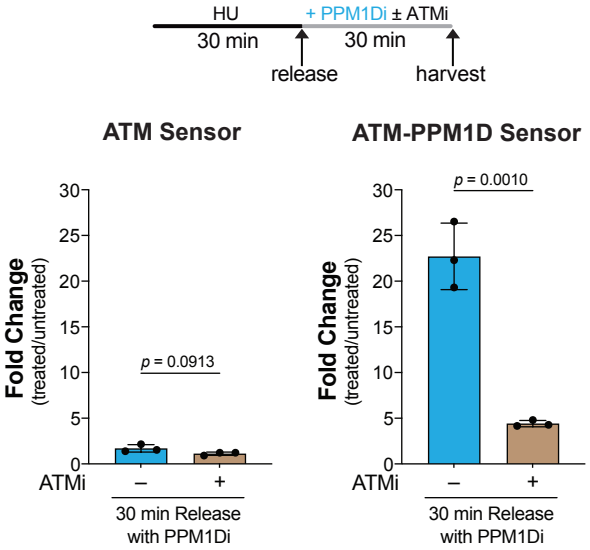
HU
30 min
+ PPM1Di ± ATMi
30 min
release
harvest
ATM Sensor
ATM-PPM1D Sensor
Fold Change
(treated/untreated)
p = 0.0913
p = 0.0010
ATMi
–
+
30 min Release
with PPM1Di